

PREPRINT

A symmetry and Noether charge preserving discretization of initial value problems

Alexander Rothkopf^{1*} and Jan Nordström^{2,3}

*Correspondence:

alexander.rothkopf@uis.no¹Faculty of Science and Technology, University of Stavanger, 4021, Stavanger, Norway

Full list of author information is available at the end of the article

Abstract

Taking insight from the theory of general relativity, where space and time are treated on the same footing, we develop a novel geometric variational discretization for second order initial value problems (IVPs). By discretizing the dynamics along a world-line parameter, instead of physical time directly, we retain manifest translation symmetry and conservation of the associated continuum Noether charge. A non-equidistant time discretization emerges dynamically, realizing a form of automatic adaptive mesh refinement (AMR), guided by the system symmetries. Using appropriately regularized summation by parts finite difference operators, the continuum Noether charge, defined via the Killing vector associated with translation symmetry, is shown to be exactly preserved in the interior of the simulated time interval. The convergence properties of the approach are demonstrated with two explicit examples.

Keywords: Initial Value Problem, Summation By Parts, Time-Translation Invariance, Conserved Noether Charge, Adaptive Mesh Refinement

1 Introduction

Symmetries play a central role in our understanding of dynamical processes in both classical [1, 2] and quantum [3] physics. Emmy Noether achieved groundbreaking insight, when she proved that the presence of a global continuous symmetry in the action \mathcal{S} of a system implies the existence of a conserved current, whenever the equations of motions are fulfilled [4]. Via such a Noether current, one can define a quantity, which remains unchanged during the evolution of the system and which is referred to as Noether charge. Noether's theorem thus offers a fundamental understanding of central tenets of classical physics, such as energy and momentum conservation, which it relates to the invariance of physics under translations in time and space respectively.

In quantum theory, the presence of symmetries limits the type of quantum fluctuations which may occur [3], with measurable consequences for the spectrum of elementary particles and their bound states. The four Noether currents associated with space and time translations are conventionally summarized in a quantity called the energy-momentum tensor $T^{\mu\nu}(x)$, where μ and ν refer to spatial and temporal components. It offers access to vital properties of a system, one pertinent example being the energy density profile [5] of a static charge distribution via the

$\varepsilon(x) = T^{00}(x)$ component or the corresponding electric field-line configuration via the spatial components $T_{ij}(x) = F_{i\mu}F_j^\mu - \frac{1}{4}\delta_{ij}F_{\mu\nu}^2$ of the electromagnetic field $F_{\mu\nu}$, referred to as the Maxwell stress tensor (see e.g. [6]).

The simulation of dynamical phenomena in classical and quantum systems is often performed after discretizing space and time on a finite mesh (for a discussion of discretization in functional spaces see e.g [7]). Finite difference schemes, formulated in their modern summation-by-parts (SBP) form (for reviews see e.g. [8–10]) offer both conceptual and practical benefits. The SBP approach in both space and time [10–12] offers proofs of stability based on the so-called energy method, which can be extended to high-order schemes in a straight forward fashion. Not only do SBP operators mimic integration by parts (IBP) exactly in the discretized setting, but in addition they constitute a cost effective approximation to differential operators on many mesh types.

The discretization of space and time in its conventional form, i.e. considering x and t as independent variables, necessarily affects the symmetry properties of the system at hand (see e.g. the discussion in [13]). Where the continuum theory e.g. admits translations of any magnitude, i.e. in particular also infinitesimal ones, the discretized theory on a space-time mesh with grid spacing Δ_μ only allows one to shift space and time by that finite amount. In general this entails that a central condition of Noether’s theorem, the presence of a *continuous* symmetry, does not hold and the corresponding continuum Noether charge fails to remain constant over time. This is particularly concerning with regards to time translation symmetry and energy conservation, which are closely related to the stability of the simulation.

Artificial loss of energy is often considered benign, as it is simply a matter of loosing accuracy. An artificial increase of energy will, as energy is not bounded from above, eventually lead to a divergence of the simulated dynamics, characteristic of an unstable scheme. On the other hand, if energy is conserved, it puts stringent bounds on the growth of the solution. In the context of symplectic schemes, which conserve energy on average, one can relate energy conservation directly to the stability of the numerical scheme (see e.g. [14] and also [15]).

One strategy to retain energy conservation for systems with second order governing equations is to go over to a Hamiltonian approach, where only space is discretized, while time remains continuous. One converts the equation of motion of the Lagrange formalism, which is second order in the time derivative into a set of two equations of motion of first order, after replacing velocities with the so-called canonical momentum. After this step, a discrete phase-space volume preserving time stepping may be implemented (c.f. Verlet-Størmer [16]). This approach crucially hinges on the availability of a Hamiltonian picture, i.e. whether the canonical momenta can be defined, which may face difficulties in systems with inherent constraints or requires the choice of a particular gauge, as in Maxwell’s electrodynamics [17]. Another strategy is to determine whether Noether’s theorem may be salvaged in the presence of a finite grid spacing [18]. One may e.g. consider modifications to the continuum energy expression, which remain conserved, given a particular choice of difference approximation. However, as the necessary schemes are not of SBP type, they do not mimic other relevant properties of the continuum theory.

In this study we develop a generic approach to discretize second order IVPs on the level of the system Lagrangian, while retaining the manifest translation invariance

of the continuum theory. In order to do so we will take inspiration from the general theory of relativity (for a textbook see e.g. [19]), where *space and time are treated on the same footing*. In this formalism the presence of translation symmetry is evident from the form of the Lagrangian itself. We build upon our prior work on formulating IVPs directly via the action of the system, which allows us to avoid the need to derive their equation of motion. The action of the system is discretized using SBP finite difference operators with a physical null-space, developed in our previous paper [20]. These operators are crucial in mimicking the continuum derivation of Noether's theorem (and if one wishes to do so, the equations of motion).

The central outcome of this proof-of-principle study is a prescription of how to discretize second order IVPs directly on the level of the Lagrangian, while retaining the continuum time translation symmetry and thus exact conservation of the corresponding Noether charge. No reference to a Hamiltonian is required. We observe that a non-equidistant discretization emerges in the time coordinate, which represents a form of automatic adaptive mesh refinement (AMR) [21–23], guided by the inherent symmetries of the system. Our results open up a novel route for obtaining optimal AMR procedures, where clustering and coarsening emerge as part of the solution process, thus avoiding the conventional use of sensors (see e.g. [24]), adjoint techniques (see e.g. [25, 26]) or error estimates (see e.g. [27–29]).

In section 2 we discuss the continuum formulation of our geometrized variational approach with time considered as dependent variable. In section 3 the discretized formalism is introduced and we present its efficacy in section 4 using different example systems. We close with a summary and outlook in section 5.

2 Continuum formalism with manifest translation symmetry

The common starting point for the formulation of the variational principle in classical point mechanics is to consider the dynamics of a system as boundary value problem (BVP). The system, which takes on position x_i at t_i evolves to position x_f at t_f and we wish to determine the trajectory it follows. Obviously this formulation is not causal, as we already need to know the end-point of the dynamics to determine the trajectory. As discussed in [30] and in our previous study [20] it is possible to formulate the variational problem as a genuine initial value problem through a doubling of the degrees of freedom of the system.

In order to focus on the qualitatively novel ingredients of our variational approach, we first introduce it in the standard context of point mechanics as a BVP. The implementation for a genuine IVP is given in the subsequent subsection.

2.1 Boundary value problem formulation

Symmetry is a central mathematical pillar of the theory of relativity. In the special theory of relativity one formulates the laws of physics in a way that remains invariant under so-called Lorentz transformations of the coordinates, while in general relativity one constructs a description, which is invariant under an even larger class of transformations. Such a theory, invariant under arbitrary differentiable coordinate transformations, is called reparametrization invariant.

Reparameterization invariance is achieved by considering both space and time as dynamical degrees of freedom. In this study we are not interested in determining the

dynamical evolution of space-time itself but will simply borrow this reparametrization invariant formalism of general relativity for our purposes of obtaining a symmetry preserving discretization. As our prime example, we set out to describe the dynamics of a point mass in the presence of a potential. The first step is to convert this physics question into a purely geometric problem.

In general relativity, the trajectory of a particle, traveling freely in (a not necessarily flat) space-time described by the metric tensor $g_{\mu\nu}$, is given by a path that generalizes the notion of the shortest path on the corresponding space-time manifold. This path is called a geodesic. While the particle may move in a $(1 + d)$ dimensional space-time with d space and one time direction, its path traces out a one-dimensional submanifold, which we can parameterize with a single, so called world-line parameter, denoted in the following by γ . We will restrict ourselves here to two dimensions, i.e. $d = 1$, a system with one spatial and one temporal direction expressed in coordinates as $\mathbf{x}(\gamma) = (t(\gamma), x(\gamma))$.

A geodesic may be obtained from a variational principle [31], which asks for the critical point of the following action functional that measures the length of the path between two space-time points $\mathbf{x}(\gamma_i)$ and $\mathbf{x}(\gamma_f)$

$$\mathcal{S} = \int_{\gamma_i}^{\gamma_f} d\gamma (-mc) \sqrt{g_{\mu\nu} \frac{dx^\mu}{d\gamma} \frac{dx^\nu}{d\gamma}}, \quad \mathbf{x}(\gamma_i) = \mathbf{x}_i, \quad \mathbf{x}(\gamma_f) = \mathbf{x}_f. \quad (1)$$

Here Einstein's summation convention has been adopted and we have included the dimensionful prefactor mc , which, as we will show explicitly below, allows us to recover the usual action in the non-relativistic limit from eq. (1).

We refer to time $t(\gamma)$ as the zeroth component x^0 of the vector \mathbf{x} and to the spatial coordinate $x(\gamma)$ as the first component x^1 . Note that this functional is reparametrization invariant under any differentiable redefinition of the parameter γ . I.e. when converting from $\gamma \rightarrow \gamma'$ the conversion of differentials under the square root produces terms $d\gamma'/d\gamma$ that cancel with the conversion factor of the measure.

The geodesics of flat space-time, described by the diagonal metric tensor $g = \text{diag}[c^2, -1]$, which arise from the critical point of the action functional

$$\mathcal{S}_{\text{flat}} = \int_{\gamma_i}^{\gamma_f} d\gamma (-mc) \sqrt{c^2 \left(\frac{dt}{d\gamma}\right)^2 - \left(\frac{dx}{d\gamma}\right)^2}, \quad (2)$$

are straight lines, which are traversed with constant speed (see chapter 3.4 of [32]), in agreement with Newtonian mechanics.

It is important to note that while our intuition of the concept of shortest path relies on geometries with positive definite metrics (Riemannian geometry), physical spacetime, as confirmed by experiment, has a metric with both positive and negative eigenvalues (pseudo-Riemannian geometry). In such a geometry the shortest path between two points can denote a saddle point of the action functional instead of a genuine minimum, as the temporal and spatial components enter relation (1) with opposite sign.

To describe the presence of an external force acting on a point particle in flat spacetime, one conventionally amends the action $\mathcal{S}_{\text{flat}}$ simply by adding the potential term $V(x)$ responsible for generating that force (see chapter 7.9 in [1]).

Let us now discuss how we can exploit the formalism of general relativity to re-express the evolution of a particle in flat spacetime in the presence of an external force, instead as an evolution of a free particle in a non-flat spacetime. In the presence of an external force, encoded in a potential term $V(x)$, the particle trajectory in flat space-time will deviate from the straight line. A standard procedure in the study of weak-field gravity is to reinterpret the change in the particle trajectory due to a potential, instead, as the effect of a non-flat space-time without a potential present (see e.g. chapter 8 of [33]). This reinterpretation is possible, as long as the values of the potential are smaller than the rest energy (mc^2) of the point mass, a condition which is very well fulfilled for the non-relativistic systems we are interested in solving.

As we will see in the following, one can introduce the effects of a potential $V(x)$ on a point particle with mass m in the weak-field limit of general relativity by modifying the temporal component g_{00} of the diagonal metric tensor

$$g_{00} = c^2 + 2V(x)/m, \quad (3)$$

while keeping $g_{11} = -1$. I.e. one endows the metric with a non-trivial dependence on the spatial coordinate, trading the absence of an explicit external force for a non-flat spacetime.

Let us now show that such a modification of the metric indeed recovers the non-relativistic action of a particle in the presence of the potential $V(x)$. To this end we insert the modified metric eq. (3) into the geodesic action eq. (1):

$$\mathcal{S} = \int_{\gamma_i}^{\gamma_f} d\gamma (-mc) \sqrt{g_{00} \left(\frac{dt}{d\gamma}\right)^2 - \left(\frac{dx}{d\gamma}\right)^2} \quad (4)$$

$$\stackrel{g_{00} > 0}{=} \int_{\gamma_i}^{\gamma_f} d\gamma (-mc) \sqrt{g_{00} \left(\frac{dt}{d\gamma}\right)^2 \underbrace{\left[1 - \frac{1}{g_{00}} \left(\frac{dx}{d\gamma}\right)^2 \left(\frac{dt}{d\gamma}\right)^{-2}\right]}_{(dx/dt)^2}} \quad (5)$$

$$\stackrel{\frac{dx}{dt}^2 \ll g_{00} \sim c^2}{=} \int_{\gamma_i}^{\gamma_f} d\gamma \left| \frac{dt}{d\gamma} \right| (-mc) \sqrt{g_{00} \left(1 - \frac{1}{2} \frac{1}{g_{00}} \left(\frac{dx}{d\gamma}\right)^2 \left(\frac{dt}{d\gamma}\right)^{-2} + \mathcal{O}\left(\frac{1}{g_{00}^2} \left(\frac{dx}{dt}\right)^4\right)\right)} \quad (6)$$

$$\stackrel{V/m \ll c^2}{=} \int_{\gamma_i}^{\gamma_f} d\gamma \frac{dt}{d\gamma} \left(-mc^2 + \frac{1}{2} m \left(\frac{dx}{d\gamma}\right)^2 \left(\frac{dt}{d\gamma}\right)^{-2} - V(x) + \mathcal{O}\left(\left(\frac{V}{mc^2}\right)^2\right) + \mathcal{O}\left(\frac{1}{c^2} \left(\frac{dx}{dt}\right)^4\right) \right) \quad (7)$$

$$= \int_{t_i}^{t_f} dt \left(-mc^2 + \frac{1}{2} m \left(\frac{dx}{dt}\right)^2 - V(x) \right). \quad (8)$$

In the third line we have expanded the rightmost square root in eq. (5), assuming that the square of the physical velocity $(dx/dt)^2$ is much smaller than g_{00} , which is to say that the particle velocity dx/dt itself is much smaller than the speed of light c . To go from the third to the fourth line, we have in addition assumed that the potential is much smaller than the rest energy of the point particle, which allows us to expand the term $\sqrt{g_{00}} = \sqrt{c^2 + 2V(x)/m}$ in terms of $V(x)/mc^2$. We will look

for solutions where time flows forward and thus have dropped the absolute value around $dt/d\gamma$ at the beginning of the second to last line. Note that eq. (8) is nothing but the standard non-relativistic action [1] for a point particle in the presence of an arbitrary potential term with the rest energy mc^2 included.

We have thus successfully related the (artificially constructed) fully geometric description of the particle in a non-flat spacetime in eq. (5) with the standard description of a particle propagating in flat spacetime in the presence of an external potential in eq. (8) in the non-relativistic limit.

We see in eq. (8) that time emerges naturally as the independent variable in which the action integral is formulated. Of course, choosing time as independent variable hides the inherent reparametrization invariance, which persists even in the non-relativistic limit in eq. (7). Interestingly it turns out that eq. (7) is a generalization of the ad-hoc construction of a reparametrization invariant non-relativistic action, discussed in standard textbooks on the calculus of variations (see e.g. [31]). Equation (7) includes the rest mass term $-mc^2(dt/d\gamma)$, which is missing in the standard derivation and which in the absence of a potential contributes a dependence on $(dt/d\gamma)$ that plays a role in obtaining a well-defined critical point for the time degree of freedom.

The reward for our efforts lies in the fact that eq. (4) is manifestly invariant under the space-time symmetries of our $(1+1)$ dimensional system. If $V(x) = 0$ only the derivatives $dt/d\gamma$ and $dx/d\gamma$ but not t and x itself appear in the action functional eq. (1). In turn adding a constant shift to either t or x as in $\mathbf{x} \rightarrow \mathbf{x} + \mathbf{s}$ leaves the action invariant. In the presence of a spatially dependent potential $V(x)$, $g_{00}(x)$ too becomes dependent on space x and only time translation invariance remains (as the force induced by $V(x)$ changes the momentum of the point particle).

Proving time translation invariance in the conventional action eq. (8) is much more involved, as one needs to consider how x as a function of t changes under such translations and in addition the boundaries of the action integral themselves are affected by the shift. None of these complications arise in eq. (4)^[1].

In the calculus of variations it is known that the critical point of the action \mathcal{S} can be obtained by solving certain differential equations, the so called geodesic equations [31]. It follows from considering the variation of the action in all of its dependent variables t , $\dot{t} = dt/d\gamma$, x and $\dot{x} = dx/d\gamma$

$$\delta\mathcal{S}[t, \dot{t}, x, \dot{x}] = \int_{\gamma_i}^{\gamma_f} d\gamma \left\{ \frac{\partial\mathcal{L}}{\partial t} \delta t + \frac{\partial\mathcal{L}}{\partial \dot{t}} \delta \dot{t} + \frac{\partial\mathcal{L}}{\partial x} \delta x + \frac{\partial\mathcal{L}}{\partial \dot{x}} \delta \dot{x} \right\} \quad (9)$$

$$= \int_{\gamma_i}^{\gamma_f} d\gamma \left\{ \left(\frac{\partial\mathcal{L}}{\partial t} - \frac{d}{d\gamma} \frac{\partial\mathcal{L}}{\partial \dot{t}} \right) \delta t + \left(\frac{\partial\mathcal{L}}{\partial x} - \frac{d}{d\gamma} \frac{\partial\mathcal{L}}{\partial \dot{x}} \right) \delta x \right\} \quad (10)$$

$$+ \left[\frac{\partial\mathcal{L}}{\partial \dot{t}} \delta t \right]_{\gamma_i}^{\gamma_f} + \left[\frac{\partial\mathcal{L}}{\partial \dot{x}} \delta x \right]_{\gamma_i}^{\gamma_f}. \quad (11)$$

^[1]That the derivatives of space and time occur in eq. (4) as squares under the square root with a relative minus sign (hiding in g_{11}) also entails that the action is manifestly invariant under so called Lorentz boosts. These transformations mix space and time components and are related to changes between inertial coordinate systems.

where in the second line we have integrated by parts. As we are considering the variational problem as boundary value problem with the coordinates t and x fixed at the start and end points of the trajectory $\mathbf{x}(\gamma_i) = \mathbf{x}_i, \mathbf{x}(\gamma_f) = \mathbf{x}_f$, also the variations δt and δx on the boundary vanish and so do the two boundary terms above. Note that we consider t and x as distinct degrees of freedom, so that the terms in the parentheses, multiplying the arbitrary variations δx and δt , must vanish each independently at the stationary point $\delta \mathcal{S} = 0$.

By deriving the Euler-Lagrange equations of the system in the spirit of the standard BVP treatment of classical mechanics, the above derivation tells us that we may locate the classical trajectory of a non-relativistic particle under the influence of a potential, by finding the critical point of the action eq. (1) with modified g_{00} component of the metric, while keeping the start and end coordinates $\mathbf{x}(\gamma_i)$ and $\mathbf{x}(\gamma_f)$ fixed.

Note that there exist infinitely many different parameterizations of the trajectory described by $\delta \mathcal{S} = 0$, which all differ by the velocity in γ , in which this trajectory is traversed. In practice these different stationary points of \mathcal{S} lead to difficulties in numerical optimization and we therefore follow the standard practice (see e.g. discussion in [34] or [32]) of selecting a particular parameterization by choosing instead of \mathcal{S} the variations of the functional

$$\mathcal{E}_{\text{BVP}} = \int_{\gamma_i}^{\gamma_f} d\gamma E_{\text{BVP}}[t, \dot{t}, x, \dot{x}] = \int_{\gamma_i}^{\gamma_f} d\gamma \frac{1}{2} \left(g_{00} \left(\frac{dt}{d\gamma} \right)^2 + g_{11} \left(\frac{dx}{d\gamma} \right)^2 \right). \quad (12)$$

It differs from \mathcal{S} via squaring the integrand and replacing the pre-factor $-mc$ by $1/2$. These are both irrelevant changes with respect to the classical equation of motion. Since \mathcal{E}_{BVP} and \mathcal{S} differ by a monotonous function applied to their integrands, formally the same critical point ensues. I.e. the variation of \mathcal{E}_{BVP} is given by $\delta \mathcal{L} = \delta \sqrt{E_{\text{BVP}}} = \frac{\delta E_{\text{BVP}}}{2\sqrt{E_{\text{BVP}}}} = 0$, so that the trajectory that extremizes \mathcal{E}_{BVP} agrees with that for \mathcal{S} at the critical point. Note that the functional \mathcal{E}_{BVP} is not reparametrization invariant anymore. The derivative terms enter quadratically, and produce a conversion factor $(d\gamma'/d\gamma)^2$, which cannot be absorbed by the measure $d\gamma$ alone.

Let us compute the Euler-Lagrange equations (the geodesic equations) for time t and space x following from the variation of eq. (12)

$$\begin{aligned} & \delta \mathcal{E}_{\text{BVP}}[t, \dot{t}, x, \dot{x}] \\ &= \int_{\gamma_i}^{\gamma_f} d\gamma \left\{ \frac{\partial E_{\text{BVP}}}{\partial t} \delta t + \frac{\partial E_{\text{BVP}}}{\partial \dot{t}} \delta \dot{t} + \frac{\partial E_{\text{BVP}}}{\partial x} \delta x + \frac{\partial E_{\text{BVP}}}{\partial \dot{x}} \delta \dot{x} \right\} \end{aligned} \quad (13)$$

$$= \int_{\gamma_i}^{\gamma_f} d\gamma \left\{ \left(\frac{\partial E_{\text{BVP}}}{\partial t} - \frac{d}{d\gamma} \frac{\partial E_{\text{BVP}}}{\partial \dot{t}} \right) \delta t + \left(\frac{\partial E_{\text{BVP}}}{\partial x} - \frac{d}{d\gamma} \frac{\partial E_{\text{BVP}}}{\partial \dot{x}} \right) \delta x \right\} \quad (14)$$

$$+ \left[\frac{\partial E_{\text{BVP}}}{\partial \dot{t}} \delta t \right]_{\gamma_i}^{\gamma_f} + \left[\frac{\partial E_{\text{BVP}}}{\partial \dot{x}} \delta x \right]_{\gamma_i}^{\gamma_f}. \quad (15)$$

As the above boundary terms vanish, we are left with evaluating the individual expressions appearing in the parentheses of eq. (14). Below we evaluate each of

these terms individually

$$\frac{\partial E_{\text{BVP}}}{\partial t} = 0, \quad \frac{\partial E_{\text{BVP}}}{\partial \dot{t}} = g_{00}(x) \frac{dt}{d\gamma}, \quad (16)$$

$$\frac{\partial E_{\text{BVP}}}{\partial x} = \frac{1}{2} \frac{\partial g_{00}(x)}{\partial x} \left(\frac{dt}{d\gamma} \right)^2, \quad \frac{\partial E_{\text{BVP}}}{\partial \dot{x}} = g_{11} \frac{dx}{d\gamma} = -\frac{dx}{d\gamma}, \quad (17)$$

making explicit the ingredients to the geodesic equations for the temporal and spatial degrees of freedom

$$\frac{d}{d\gamma} \left(g_{00} \frac{dt}{d\gamma} \right) = 0, \quad (18)$$

$$\frac{d}{d\gamma} \left(\frac{dx}{d\gamma} \right) + \frac{1}{2} \frac{\partial g_{00}}{\partial x} \left(\frac{dt}{d\gamma} \right)^2 = 0. \quad (19)$$

The attentive reader will have recognized that eq. (18) constitutes a conservation equation for the expression inside the parenthesis. In the next chapter we will show that this quantity indeed is the conserved charge associated with the time translation symmetry of our system. In general the geodesic equations do not single out the conserved quantities in such a simple fashion. There however exists an systematic procedure to identify the space-time symmetries of the system in the form of different so-called Killing vectors, each of which leads to one conserved quantity (see section 2.2).

Note that the geodesic equations eqs. (18) and (19) are often written in a more concise fashion in the general relativity literature (see e.g. [19]). They are expressed for a general metric using the so-called Christoffel symbols $\Gamma_{\mu\nu}^{\alpha} = \frac{1}{2} g^{\alpha\beta} (\partial g_{\beta\mu} / \partial x_{\nu} + \partial g_{\beta\nu} / \partial x_{\mu} - \partial g_{\mu\nu} / \partial x_{\beta})$, where $g^{\alpha\beta}$ refers to the components of the inverse of the metric $g_{\alpha\beta}$. One obtains in short hand notation with Einstein summation implied

$$\frac{d^2 x^{\alpha}}{d\gamma^2} + \Gamma_{\mu\nu}^{\alpha} \frac{dx^{\mu}}{d\gamma} \frac{dx^{\nu}}{d\gamma} = 0. \quad (20)$$

It is important to note that the derivation of the above expression involves application of the product rule, which in the discrete setting is not valid. Therefore even though in the continuum eqs. (18) and (19) and eq. (20) are equivalent, we will work solely with the former, as only integration by parts (which is exactly mimicked by summation by parts) has been used in their derivation.

2.2 Conserved quantities, Noether's theorem and stability

Conservation of momentum and energy in general relativity is conceptually more involved compared to flat space-time, since the comparison of two quantities at different space-time points becomes a non-trivial operation due to the effects of a non-flat metric. However there may exist a vector field $K^{\mu}(x)$ along which transported quantities remain constant. These vector fields are known as Killing^[2] vector fields $K^{\mu}(x)$. The Killing vector fields are generators of infinitesimal isometries of

^[2]For completeness we note that a Killing vector field K_{μ} is defined as solution to the Killing equation $\left(\frac{\partial K_{\mu}}{\partial x^{\nu}} - \Gamma_{\mu\nu}^{\alpha} K_{\alpha} \right) + \left(\frac{\partial K_{\nu}}{\partial x^{\mu}} - \Gamma_{\nu\mu}^{\alpha} K_{\alpha} \right) = 0$.

the space-time manifold. Moving all points of the manifold in the direction of the Killing field leaves the manifold unchanged.

As discussed in standard literature on general relativity (see e.g. chapter 3.8 of [32]), each Killing vector field K^μ can be used to define a conserved quantity Q_K via the expression

$$Q_K = g_{\alpha\beta} K^\alpha \dot{x}^\beta. \quad (21)$$

Computing the change of Q_K along a geodesic, parameterized by γ , one finds from combining eqs. (20) and (21) and the equation that defines the Killing vector that $dQ_K/d\gamma = 0$, i.e. it vanishes. We will give an explicit example of such a conserved quantity below.

More intuitively, one can think of the role of K^μ as pointing out directions along which the metric g of spacetime in our system remains constant. In the spirit of Noether's theorem, assume that the integrand E_{BVP} of our action functional \mathcal{E}_{BVP} in eq. (12) remains unchanged under infinitesimal translations with magnitude ϵ in the direction of K^μ . The change in coordinates under such a shift is $\delta x^\mu = \epsilon K^\mu$. Noether's theorem tells us that the conserved quantity corresponding to δx^μ is given by $J = \delta x^\mu \frac{\partial E}{\partial \dot{x}^\mu}$, which, when written explicitly as $\epsilon K^\alpha g_{\alpha\beta} \frac{dx^\beta}{d\gamma}$, turns out to just be ϵQ_K .

In case of our geometrized problem of determining the dynamics of a point particle under the influence of a potential $V(x)$, the metric remains independent of time t . Thus the vector $K_t = (1, 0)$ constitutes a Killing vector associated with time translation symmetry. The conservation of the associated conserved quantity $Q_t = K_t^\mu g_{\mu\nu} \dot{x}^\nu = g_{00} \dot{t}$ follows straight forwardly from the geodesic equation for t

$$\frac{d}{d\gamma} Q_t \stackrel{K_t = (1,0)}{\underset{\text{eq. (21)}}{=}} \frac{d}{d\gamma} (g_{00} \dot{t}) \stackrel{\text{eq. (18)}}{=} 0, \quad (22)$$

i.e. the quantity Q_t remains constant along the geodesic. Note that this quantity is different from the usual energy considered in the non-relativistic formalism.

Turning to the question of stability, let us show next that as a consequence of the presence of a conserved quantity together with the form of the geodesic equations and the reasonable assumption that the potential of the system is bounded from below, it is possible to provide an upper bound on the derivatives of the trajectories obtained as critical point of the functional eq. (12).

In an analogy to the construction of a Hamiltonian from a Lagrangian, we define the following

$$\mathcal{H}_{\text{BVP}} = \int_{\gamma_i}^{\gamma_f} d\gamma \underbrace{\frac{1}{2} \left(g_{00}(x) \left(\frac{dt}{d\gamma} \right)^2 - g_{11} \left(\frac{dx}{d\gamma} \right)^2 \right)}_{H_{\text{BVP}}}, \quad (23)$$

$$= \int_{\gamma_i}^{\gamma_f} d\gamma \frac{1}{2} \left((c^2 + 2 \frac{V(x)}{m}) \left(\frac{dt}{d\gamma} \right)^2 + \left(\frac{dx}{d\gamma} \right)^2 \right). \quad (24)$$

Due to the flipped sign in front of g_{11} , compared to the action eq. (12), this quantity is actually positive definite, as long as $V(x)$ is bounded from below^[3]. \mathcal{H}_{BVP} thus provides a norm on the function space in which $t(\gamma)$ and $x(\gamma)$ reside. Now let us inspect the evolution of the integrand H_{BVP}

$$\begin{aligned} \frac{dH_{\text{BVP}}}{d\gamma} &= \frac{1}{2} \frac{dg_{00}}{d\gamma} \left(\frac{dt}{d\gamma} \right)^2 + g_{00} \frac{dt}{d\gamma} \frac{d^2t}{d\gamma^2} + \frac{dx}{d\gamma} \frac{d^2x}{d\gamma^2}, \\ &= \frac{dx}{d\gamma} \left[\frac{1}{2} \frac{\partial g_{00}}{\partial x} \left(\frac{dt}{d\gamma} \right)^2 + \frac{d^2x}{d\gamma^2} \right] + g_{00} \frac{dt}{d\gamma} \frac{d^2t}{d\gamma^2}, \\ &\stackrel{\text{eq. (19)}}{=} \underbrace{g_{00}}_{Q_t \text{ const.}} \frac{dt}{d\gamma} \frac{d^2t}{d\gamma^2}. \end{aligned} \quad (25)$$

To arrive at the final expression in eq. (25), we use the fact that one can rewrite $dg_{00}/d\gamma = (\partial g_{00}(x)/\partial x)\dot{x}$ and combine the first and third term to apply eq. (19). This simplification tells us that the change in H_{BVP} is given solely by the second derivative of time with respect to the world-line parameter. Now we can integrate up twice $\mathcal{H}_{\text{BVP}} = \int_{\gamma_i}^{\gamma_f} d\gamma \int_{\gamma_i}^{\gamma} d\gamma' (dH_{\text{BVP}}(\gamma')/d\gamma')$ to get

$$\begin{aligned} \mathcal{H}_{\text{BVP}} &= mg_{00}(x_i) \dot{t}(\gamma_i) \int_{\gamma_i}^{\gamma_f} d\gamma (\dot{t}(\gamma) - \dot{t}(\gamma_i)), \\ &= g_{00}(x_i) \dot{t}(\gamma_i) \left(-\dot{t}(\gamma_i)(\gamma_f - \gamma_i) + (t(\gamma_f) - t(\gamma_i)) \right), \\ &\leq g_{00}(x_i) \dot{t}(\gamma_i) (t(\gamma_f) - t(\gamma_i)). \end{aligned} \quad (26)$$

For the last inequality we use the fact that the world-line is parameterized by an increasing γ and correspondingly time moves forward along the world-line.

In the BVP setting, where both $t(\gamma_i)$ and $t(\gamma_f)$ are given apriori, eq. (26) constitutes a proof that the norm \mathcal{H}_{BVP} defined on the derivatives of the solution t and x grows at most linearly with time, precluding the occurrence of exponentially increasing behavior that would signal an instability, in turn establishing stability of the geometric approach.

2.3 Initial value formulation

So far we have shown how the geodesic equations eqs. (18) and (19) can be obtained from a variational principle formulated as a boundary value problem in time. However for a causal description as an initial value problem, we must be able to determine the dynamics of the particle without knowledge of the final point of the trajectory. If one wishes to prescribe only initial values, i.e. positions and derivatives at γ_i , then the variations δx^μ in eq. (9) do not vanish at the end of the particle world line, i.e. at γ_f . In turn the equivalence between the critical point of \mathcal{S} and the Euler-Lagrange equations in eq. (10) does not hold. As discussed by [30] and put into practice in our previous publication [20] one can overcome this issue by constructing an action with doubled degrees of freedom, living on a closed contour with a forward and backward branch in γ .

^[3]Since physical forces arise from the derivative of the potential, we may always add a constant to a bounded potential that will make g_{00} positive.

Since both time and space constitute dependent degrees of freedom in our approach, we need to introduce both forward and backward variants of each of them $x_1(\gamma), x_2(\gamma)$ and $t_1(\gamma), t_2(\gamma)$. The degrees of freedom on the forward contour enter the action functional with the usual Lagrangian, while those on the backward contour are assigned the negative Lagrangian. Choosing to build the doubled formalism based on the action \mathcal{E}_{BVP} we obtain

$$\mathcal{E}_{\text{IVP}} = \int_{\gamma_i}^{\gamma_f} d\gamma E_{\text{IVP}}[t_1, \dot{t}_1, x_1, \dot{x}_1, t_2, \dot{t}_2, x_2, \dot{x}_2], \quad (27)$$

$$= \int_{\gamma_i}^{\gamma_f} d\gamma \left\{ E_{\text{BVP}}[t_1, \dot{t}_1, x_1, \dot{x}_1] - E_{\text{BVP}}[t_2, \dot{t}_2, x_2, \dot{x}_2] \right\}. \quad (28)$$

As discussed in detail in [20], the inner workings of the doubled formalism become more transparent, once we go over to expressing the action \mathcal{E}_{IVP} in terms of the central and difference coordinates $x_+ = \frac{1}{2}(x_1 + x_2)$ and $x_- = x_1 - x_2$ and $t_+ = \frac{1}{2}(t_1 + t_2)$ and $t_- = t_1 - t_2$ respectively. The variation now proceeds in the independent degrees of freedom x_{\pm} and t_{\pm} and yields

$$\begin{aligned} \delta\mathcal{E}_{\text{IVP}}[t_{\pm}, \dot{t}_{\pm}, x_{\pm}, \dot{x}_{\pm}] &= \\ & \int_{\gamma_i}^{\gamma_f} d\gamma \left\{ \frac{\partial E_{\text{IVP}}}{\partial t_+} \delta t_+ + \frac{\partial E_{\text{IVP}}}{\partial \dot{t}_+} \delta \dot{t}_+ + \frac{\partial E_{\text{IVP}}}{\partial t_-} \delta t_- + \frac{\partial E_{\text{IVP}}}{\partial \dot{t}_-} \delta \dot{t}_- \right. \\ & \quad \left. + \frac{\partial E_{\text{IVP}}}{\partial x_+} \delta x_+ + \frac{\partial E_{\text{IVP}}}{\partial \dot{x}_+} \delta \dot{x}_+ + \frac{\partial E_{\text{IVP}}}{\partial x_-} \delta x_- + \frac{\partial E_{\text{IVP}}}{\partial \dot{x}_-} \delta \dot{x}_- \right\} \\ &= \int_{\gamma_i}^{\gamma_f} d\gamma \left\{ \left(\frac{\partial E_{\text{IVP}}}{\partial t_+} - \frac{d}{d\gamma} \frac{\partial E_{\text{IVP}}}{\partial \dot{t}_+} \right) \delta t_+ + \left(\frac{\partial E_{\text{IVP}}}{\partial t_-} - \frac{d}{d\gamma} \frac{\partial E_{\text{IVP}}}{\partial \dot{t}_-} \right) \delta t_- \right. \\ & \quad \left. + \left(\frac{\partial E_{\text{IVP}}}{\partial x_+} - \frac{d}{d\gamma} \frac{\partial E_{\text{IVP}}}{\partial \dot{x}_+} \right) \delta x_+ + \left(\frac{\partial E_{\text{IVP}}}{\partial x_-} - \frac{d}{d\gamma} \frac{\partial E_{\text{IVP}}}{\partial \dot{x}_-} \right) \delta x_- \right\} \\ & \quad + \left[\frac{\partial E_{\text{IVP}}}{\partial \dot{t}_+} \delta t_+ \right]_{\gamma_i}^{\gamma_f} + \left[\frac{\partial E_{\text{IVP}}}{\partial \dot{t}_-} \delta t_- \right]_{\gamma_i}^{\gamma_f} + \left[\frac{\partial E_{\text{IVP}}}{\partial \dot{x}_+} \delta x_+ \right]_{\gamma_i}^{\gamma_f} + \left[\frac{\partial E_{\text{IVP}}}{\partial \dot{x}_-} \delta x_- \right]_{\gamma_i}^{\gamma_f}. \end{aligned} \quad (29)$$

$$(30)$$

To arrive at eq. (30) we have carried out four integrations by parts. As the next step, we consider under which conditions the boundary terms in the above expression vanish. Since we prescribe fixed initial values for both time and space, the variations $\delta t_{\pm}(\gamma_i) = 0$ and $\delta x_{\pm}(\gamma_i) = 0$ vanish. What about the variations at the end of the forward and backward world-line? As long as we require that

$$x_2(\gamma_f) = x_1(\gamma_f), \quad t_2(\gamma_f) = t_1(\gamma_f), \quad (31)$$

it follows that $\delta x_-(\gamma_f)$ and $\delta t_-(\gamma_f)$ vanish and with it the corresponding boundary terms. The only remaining terms are those at γ_f which feature δx_+ and δt_+ . As these variations do not vanish, we instead inspect the terms multiplying them, i.e. $\partial E_{\text{IVP}}/\partial \dot{t}_+$ and $\partial E_{\text{IVP}}/\partial \dot{x}_+$. Using the definition $x_1 = x_+ + \frac{1}{2}x_-$ and $x_2 = x_+ - \frac{1}{2}x_-$

and correspondingly for $t_{1,2}$, we find from the defining equation for E_{IVP} eq. (12)

$$\begin{aligned} \frac{dE_{\text{IVP}}}{d\dot{x}_+} &= \frac{\partial E_{\text{IVP}}[t_{1,2}, \dot{t}_{1,2}, x_{1,2}, \dot{x}_{1,2}]}{\partial \dot{x}_1} \frac{d\dot{x}_1}{d\dot{x}_+} + \frac{\partial E_{\text{IVP}}[t_{1,2}, \dot{t}_{1,2}, x_{1,2}, \dot{x}_{1,2}]}{\partial \dot{x}_2} \frac{d\dot{x}_2}{d\dot{x}_+}, \\ &= \frac{\partial E_{\text{BVP}}[t_1, \dot{t}_1, x_1, \dot{x}_1]}{\partial \dot{x}_1} \frac{d\dot{x}_1}{d\dot{x}_+} - \frac{\partial E_{\text{BVP}}[t_2, \dot{t}_2, x_2, \dot{x}_2]}{\partial \dot{x}_2} \frac{d\dot{x}_2}{d\dot{x}_+}, \end{aligned} \quad (32)$$

$$= g_{11}(x_1)\dot{x}_1 - g_{11}(x_2)\dot{x}_2 = -\dot{x}_1 + \dot{x}_2. \quad (33)$$

Similarly one obtains

$$\frac{dE_{\text{IVP}}}{d\dot{t}_+} = g_{00}(x_1)\dot{t}_1 - g_{00}(x_2)\dot{t}_2. \quad (34)$$

Together with condition eq. (31) that the values of $x_{1,2}$ and $t_{1,2}$ must agree at γ_f , this result tells us that in order for the two remaining boundary terms to vanish, we need to also identify the derivatives of $x_{1,2}$ and $t_{1,2}$ at the point γ_f

$$\dot{x}_2(\gamma_f) = \dot{x}_1(\gamma_f), \quad \dot{t}_2(\gamma_f) = \dot{t}_1(\gamma_f). \quad (35)$$

Note that we have now managed to remove the boundary terms without the need for specifying the concrete value of t 's and x 's at the final point γ_f . This is the central contribution of the forward-backward construction.

The last remaining step is to undo the proliferation of degrees of freedom that occurred when introducing the forward-backward construction. It has been shown [30, 35] that taking the so-called physical limit achieves this goal, where the constraints $x_1(\gamma) - x_2(\gamma) = x_-(\gamma) = 0$ and $t_1(\gamma) - t_2(\gamma) = t_-(\gamma) = 0$ are enforced. The remaining x_+ and t_+ are identified with the true classical geodesics.

In terms of the Euler-Lagrange equations in parentheses in eq. (30)

$$\frac{\partial E_{\text{IVP}}}{\partial x_{\pm}} - \frac{d}{d\gamma} \frac{\partial E_{\text{IVP}}}{\partial \dot{x}_{\pm}} = 0, \quad \frac{\partial E_{\text{IVP}}}{\partial t_{\pm}} - \frac{d}{d\gamma} \frac{\partial E_{\text{IVP}}}{\partial \dot{t}_{\pm}} = 0, \quad (36)$$

the physical limit entails that only those equations independent of x_- and t_- survive. With the construction of the action $E_{\text{IVP}} = E_{\text{BVP}}[x_1, \dot{x}_1, t_1, \dot{t}_1] - E_{\text{BVP}}[x_2, \dot{x}_2, t_2, \dot{t}_2]$ from a difference of the E_{BVP} functionals, there will appear at least a linear dependence on the minus degrees of freedom. Hence in the physical limit only those Euler-Lagrange equations linear in x_- and t_- will survive, where the minus degrees of freedom have been removed by taking the derivative with respect to x_- or t_- .

Note that we have decided to not only specify the value and derivative of x at initial γ_i but also those of t . As we wish to determine the dynamics of a point particle in the presence of a potential with given $x(t_i)$ and $dx/dt(t_i)$, there remains a freedom in choosing $\dot{x}(\gamma_i)$ and $\dot{t}(\gamma_i)$, since only their ratio needs to be fixed $dx/dt(t = t_0) = \dot{x}(\gamma_i)/\dot{t}(\gamma_i)$. The end of the time interval traversed by the world line parameter γ , will consequently depend on the value prescribed to $\dot{t}(\gamma_i)$ and emerges dynamically from the combined evolution of x and t .

At this point we have formulated a manifest time translation symmetric variational principle that encodes the dynamics of a point particle evolving in the

presence of a non-relativistic potential as initial value problem. Our next goal is to discretize the action functional \mathcal{E}_{IVP} in section 3 using SBP finite difference operators. Since all derivations of the Euler-Lagrange equations, as well as that of the conserved quantity Q_t have made ample reference to integration by parts, it is paramount to use such a discretization technique, which faithfully mimics this continuum property on a finite mesh.

3 Discretized formalism for IVPs

The central novelty we introduce in this section is related to the fact that the discretization of the action functional takes place in the world-line parameter γ and not in the time variable t , as in conventional discretization prescriptions. I.e. the values of both time $t(\gamma)$ and position $x(\gamma)$ remain continuous and in turn we achieve *preservation of the continuum space-time symmetries* even after discretization.

In the presence of a potential that depends on x but not on t , the invariance under infinitesimal constant shifts in time is hence retained. This comes about, since the metric remains invariant under changes in t , which in turn leads to a simple form of the corresponding Killing equation, which shows that $K_t = (1, 0)$ indeed is a Killing vector. The symmetry of the metric under time translation is intimately related to energy conservation via Q_t and thus the stability of the simulation. In the absence of a potential, when the metric does not depend on neither t nor x , our discretized approach, in addition to $K_t = (1, 0)$, retains the continuum invariance under shifts in x via the Killing vector $K_x = (0, 1)$, as well as the invariance under boosts via the Killing vector $K_\eta = (x, t)$.

We will give numerical evidence that we achieve exact conservation of Q_t in the interior of the simulated domain, even in the case of highly non-harmonic motion. In contrast to other formally energy preserving schemes, such as the leap-frog, our approach, using SBP operators, is consistent with the continuum formulation, in that it only requires the actual initial conditions of the system at hand, avoiding the need to stagger the degrees of freedom (also known as insertion of dummy points).

After introducing the discretization on the level of the underlying action functional, we will obtain the classical trajectory by numerically finding the critical point of that functional without the need to derive the corresponding equations of motion. To make sure that the solution of the discretized variational principle mimics as accurately as possible the continuum theory, we deploy summation-by-parts finite difference operators [8–10].

Note that we are discretizing the world-line parameter γ with equidistant steps, whereas both the values of t and x arise dynamically from the evolution of the simulation along γ . I.e. a not necessarily equidistant discretization of the time coordinate emerges dynamically in our approach. As we will see in section 4 this dynamical time discretization realizes a one-dimensional form of automatic adaptive mesh refinement, guided by the symmetries of the system. I.e. the non-equidistant discretization in t plays a crucial role in guaranteeing that the Noether charge Q_t remains conserved.

Another non-standard feature of our technique is the departure from the conventional notion of carrying out a simulation on a predefined time interval. We instead provide the initial time and its velocity with respect to γ , so that the end-point of the simulation too emerges dynamically.

In the following we will consider the trajectory of a point particle propagating under the influence of an arbitrary x but not t dependent potential $V(x)$. We begin by discretizing the action functional \mathcal{E}_{IVP} of eq. (28) along the world-line parameter γ between γ_i and γ_f with N_γ steps, leading to a step-size of $d\gamma = (\gamma_f - \gamma_i)/(N_\gamma - 1)$. We will add to E_{IVP} Lagrange multipliers to explicitly account for both the initial conditions and the connecting conditions required by doubling of the degrees of freedom. The forward and backward paths $x_{1,2}$ and times $t_{1,2}$ are described by $\mathbf{x}_{1,2} = (x_{1,2}(0), x_{1,2}(\Delta\gamma), x_{1,2}(2\Delta\gamma), \dots, x_{1,2}((N_\gamma - 1)\Delta\gamma))^T$ and $\mathbf{t}_{1,2} = (t_{1,2}(0), t_{1,2}(\Delta\gamma), t_{1,2}(2\Delta\gamma), \dots, t_{1,2}((N_\gamma - 1)\Delta\gamma))^T$ respectively.

The integral in \mathcal{E}_{IVP} is approximated with a quadrature rule, consistent with our choice of finite difference operator, in the form of a diagonal positive definite matrix \mathbb{H} . The inner product on discretized paths and times thus reads $(\mathbf{x}, \mathbf{x}') = \mathbf{x}^T \mathbb{H} \mathbf{x}'$.

With integration by parts being a central element in establishing both equations of motion and the existence of conserved quantities, we must use a discretization that mimics IBP exactly, which is achieved by deploying summation-by-parts (SBP) operators \mathbb{D} with the defining properties

$$\mathbb{D} = \mathbb{H}^{-1} \mathbb{Q}, \quad \mathbb{Q}^T + \mathbb{Q} = \mathbb{E}_N - \mathbb{E}_0 = \text{diag}[-1, 0, \dots, 0, 1]. \quad (37)$$

In this study we consider both the lowest order SBP discretization scheme, referred to as **SBP21** and the next higher order scheme **SBP42**. The former is second order in the interior and exhibits one order less on the boundary. Using the trapezoidal rule for integration one has

$$\mathbb{H}^{[2,1]} = \Delta\gamma \begin{bmatrix} 1/2 & & & & \\ & 1 & & & \\ & & \ddots & & \\ & & & 1 & \\ & & & & 1/2 \end{bmatrix}, \quad \mathbb{D}^{[2,1]} = \frac{1}{2\Delta\gamma} \begin{bmatrix} -2 & 2 & & & \\ -1 & 0 & 1 & & \\ & & \ddots & & \\ & & & -1 & 0 & 1 \\ & & & & -2 & 2 \end{bmatrix}. \quad (38)$$

The **SBP42** scheme achieves fourth order accuracy in the interior, which reduces to second order on the boundary

$$\mathbb{H}^{[4,2]} = \Delta\gamma \begin{bmatrix} \frac{17}{48} & & & & & \\ & \frac{59}{48} & & & & \\ & & \frac{43}{48} & & & \\ & & & \frac{49}{48} & & \\ & & & & 1 & \\ & & & & & \ddots \end{bmatrix},$$

Using the operators defined above, we can now write the discretized action functional in the following fashion

$$\begin{aligned}
\mathbb{E}_{\text{IVP}} = & \frac{1}{2} \left\{ (\bar{\mathbb{D}}_t^R \mathbf{t}_1)^T \mathfrak{d} \left[c^2 + \frac{2\mathbf{V}(\mathbf{x}_1)}{m} \right] \bar{\mathbb{H}}(\bar{\mathbb{D}}_t^R \mathbf{t}_1) - (\bar{\mathbb{D}}_x^R \mathbf{x}_1)^T \bar{\mathbb{H}}(\bar{\mathbb{D}}_x^R \mathbf{x}_1) \right\} \\
& - \frac{1}{2} \left\{ (\bar{\mathbb{D}}_t^R \mathbf{t}_2)^T \mathfrak{d} \left[c^2 + \frac{2\mathbf{V}(\mathbf{x}_2)}{m} \right] \bar{\mathbb{H}}(\bar{\mathbb{D}}_t^R \mathbf{t}_2) - (\bar{\mathbb{D}}_x^R \mathbf{x}_2)^T \bar{\mathbb{H}}(\bar{\mathbb{D}}_x^R \mathbf{x}_2) \right\} \\
& + \lambda_1 (\mathbf{t}_1[1] - t_i) + \lambda_2 ((\mathbb{D}\mathbf{t}_1)[1] - \dot{t}_i) + \lambda_3 (\mathbf{x}_1[1] - x_i) \\
& + \lambda_4 ((\mathbb{D}\mathbf{x}_1)[1] - \dot{x}_i) \\
& + \lambda_5 (\mathbf{t}_1[N_\gamma] - \mathbf{t}_2[N_\gamma]) + \lambda_6 (\mathbf{x}_1[N_\gamma] - \mathbf{x}_2[N_\gamma]) \\
& + \lambda_7 ((\mathbb{D}\mathbf{t}_1)[N_\gamma] - (\mathbb{D}\mathbf{t}_2)[N_\gamma]) + \lambda_8 ((\mathbb{D}\mathbf{x}_1)[N_\gamma] - (\mathbb{D}\mathbf{x}_2)[N_\gamma]). \quad (42)
\end{aligned}$$

Conventional matrix vector multiplication is implied in the above expression, whenever a matrix quantity such as $\bar{\mathbb{H}}$ or $\bar{\mathbb{D}}$ acts on a vector $\mathbf{x}_{1,2}$ or $\mathbf{t}_{1,2}$. The matrix denoted by $\mathfrak{d}[f(\mathbf{x})]$ contains on its diagonal the values $\mathfrak{d}_{kk} = f(\mathbf{x}(\gamma_k))$ and zero otherwise. We deploy an appropriately modified matrix $\bar{\mathbb{H}}$ for the inner product in the presence of the affine-coordinate regularized SBP operators (see appendix A).

The initial conditions we supply are the values of the spatial and temporal coordinate x_i, t_i , as well as the initial velocities with respect to the world line parameter γ , i.e. \dot{x}_i and \dot{t}_i . Since our physical problem is formulated as an initial value problem, given t_i, x_i and the physical velocity $v_i = dx/dt$, there exists a freedom to choose \dot{t}_i and \dot{x}_i , as only their ratio is fixed $v_i = \dot{x}_i/\dot{t}_i$. We have added eight Lagrange multipliers, whose role is to explicitly implement the initial conditions (λ_{1-4}) and the connecting conditions at the end of the forward and backward branches of our doubled degree of freedom construction (λ_{5-8}).

Once the action functional has been formulated in its discrete form, changing from SBP21 to SBP42 only requires replacement of the corresponding difference operator \mathbb{D} and quadrature matrix \mathbb{H} but no further changes to the functional itself.

This concludes the description of our novel variational approach and we proceed to evaluate its properties and performance based on two concrete numerical examples.

4 Numerical results

In this section we will present explicit results for the numerically obtained classical trajectory of a point particle in the presence of two different potentials, $V_1(x) = \alpha x$ and $V_4(x) = \kappa x^4$. These two choices correspond to a model of a point mass falling in a constant gravitational field and carrying out highly-nonlinear anharmonic motion. We set the mass of the particle to unity, as well as adopt without loss of generality the convention that the speed of light $c = 1$, which simply amounts to a particular choice of units for length and time.

Let us stress again that while standard numerical methods exist to solve the equations of motion for each of these systems, the novelty of the approach presented here lies in the fact that we retain the continuum time shift invariance of the system and thus achieve *exact conservation* of Q_t in the interior of the simulated time domain. In addition we determine the classical trajectory directly from the action functional of the geometrized problem, without the need to derive the equation of motion.

We implement the action functional eq. (42) in the Mathematica language^[5]. As the critical point of the action may be a saddle point, instead of an actual minimum, we must be careful in deploying established numerical optimization algorithms in the dynamical degrees of freedom $\mathbf{d} = \{\mathbf{t}_{1,2}, \mathbf{x}_{1,2}, \lambda_{1-8}\}$. Instead of minimizing \mathbb{E}_{IVP} directly, we will minimize the Euclidean norm of the gradient $|\nabla_{\mathbf{d}}\mathbb{E}_{\text{IVP}}|^2$. Via this detour, a saddle point is converted into a minimum. In practice we deploy a chain of minimization algorithms. We start with a preconditioning based on the LBFGS quasi-Newton algorithm, which features cost efficient iteration steps, when far away from the true critical point. It is followed by further iterations based on the full Newton method, which exhibits a faster convergence rate than the LBFGS algorithm when close to the critical point. Once the critical point has been approached to at least floating point precision we switch to the interior point optimization, which showed reliable performance in identifying the critical point to any desired tolerance. For our numerical tests in Mathematica, we used `WorkingPrecision` of 40 and `PrecisionGoal` of 40.

The figures shown in the following are based on results from the `SBP21` operator and include the outcomes from the `SBP42` operators when indicated in the text.

4.1 Linear potential case

We discretize the continuous action functional

$$\begin{aligned} \mathcal{E}_{\text{IVP}}^{\text{lin}} = & \int_{\gamma_i}^{\gamma_f} d\gamma \frac{1}{2} \left\{ \left(1 + 2\alpha x_1(\gamma)\right) \left(\frac{dt_1}{d\gamma}\right)^2 - \left(\frac{dx_1}{d\gamma}\right)^2 \right\} \\ & - \int_{\gamma_i}^{\gamma_f} d\gamma \frac{1}{2} \left\{ \left(1 + 2\alpha x_2(\gamma)\right) \left(\frac{dt_2}{d\gamma}\right)^2 - \left(\frac{dx_2}{d\gamma}\right)^2 \right\} \\ & + \lambda_1(t(\gamma_i) - t_i) + \lambda_2(\dot{t}_1(\gamma_i) - \dot{t}_i) + \lambda_3(x_1(\gamma_i) - x_i) + \lambda_4(\dot{x}_1(\gamma_i) - \dot{x}_i) \\ & + \lambda_5(t_1(\gamma_f) - t_2(\gamma_2)) + \lambda_6(\dot{t}_1(\gamma_f) - \dot{t}_2(\gamma_2)) \\ & + \lambda_7(x_1(\gamma_f) - x_2(\gamma_2)) + \lambda_8(\dot{x}_1(\gamma_f) - \dot{x}_2(\gamma_2)) \end{aligned} \quad (43)$$

along the world-line of the particle motion between $\gamma_i = 0$ and $\gamma_f = 1$ with $N_\gamma = 32$ points. Without loss of generality, we arbitrarily set the starting time to $t_i = 0$ and the starting position to $x_i = 1$. To obtain an initial velocity $v_i = 1/10$ we choose $\dot{t} = 1$ and $\dot{x} = v_i$. Note that we do not fix the value of t_f but only the initial velocity of time with respect to γ . The choice of $\dot{t} = 1$ will lead to dynamics, such that t_f will be of the order of one. (In the next subsection we will also provide results for different choices of \dot{t}_i .) As strength for the linear potential we choose $\alpha = 1/4$. The

^[5]The code using both the `SBP21` or `SBP42` operator is available under open access on the Zenodo repository [37].

corresponding discrete action functional reads explicitly

$$\begin{aligned}
\mathbb{E}_{\text{IVP}}^{\text{lin}} = & \frac{1}{2} \{ (\bar{\mathbb{D}}_t^{\text{R}} \mathbf{t}_1)^{\text{T}} \text{d} [1 + 2\alpha \mathbf{x}_1] \bar{\mathbb{H}}(\bar{\mathbb{D}}_t^{\text{R}} \mathbf{t}_1) - (\bar{\mathbb{D}}_x^{\text{R}} \mathbf{x}_1)^{\text{T}} \bar{\mathbb{H}}(\bar{\mathbb{D}}_x^{\text{R}} \mathbf{x}_1) \} \\
& - \frac{1}{2} \{ (\bar{\mathbb{D}}_t^{\text{R}} \mathbf{t}_2)^{\text{T}} \text{d} [1 + 2\alpha \mathbf{x}_2] \bar{\mathbb{H}}(\bar{\mathbb{D}}_t^{\text{R}} \mathbf{t}_2) - (\bar{\mathbb{D}}_x^{\text{R}} \mathbf{x}_2)^{\text{T}} \bar{\mathbb{H}}(\bar{\mathbb{D}}_x^{\text{R}} \mathbf{x}_2) \} \\
& + \lambda_1 (\mathbf{t}_1[1] - t_i) + \lambda_2 ((\mathbb{D} \mathbf{t}_1)[1] - \dot{t}_i) \\
& + \lambda_3 (\mathbf{x}_1[1] - x_i) + \lambda_4 ((\mathbb{D} \mathbf{x}_1)[1] - \dot{x}_i) \\
& + \lambda_5 (\mathbf{t}_1[N_\gamma] - \mathbf{t}_2[N_\gamma]) + \lambda_6 (\mathbf{x}_1[N_\gamma] - \mathbf{x}_2[N_\gamma]) \\
& + \lambda_7 ((\mathbb{D} \mathbf{t}_1)[N_\gamma] - (\mathbb{D} \mathbf{t}_2)[N_\gamma]) + \lambda_8 ((\mathbb{D} \mathbf{x}_1)[N_\gamma] - (\mathbb{D} \mathbf{x}_2)[N_\gamma]). \quad (44)
\end{aligned}$$

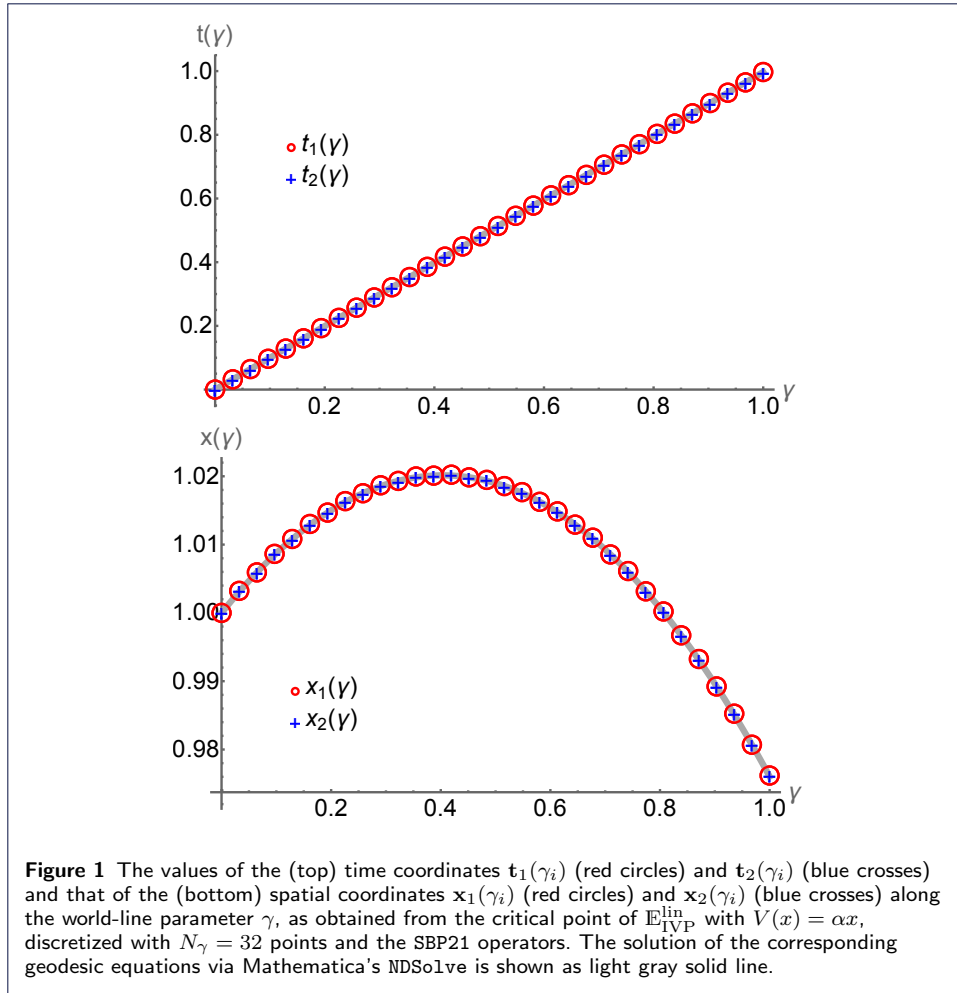
Let us take a look in fig. 1 at the raw results for the forward and backward time and spatial coordinates, as obtained from the critical point of $\mathbb{E}_{\text{IVP}}^{\text{lin}}$ with $V(x) = \alpha x$. In the top panel, we show $\mathbf{t}_1(\gamma_i)$ as red circles and $\mathbf{t}_2(\gamma_i)$ as blue crosses, while in the bottom panel these symbols denote the spatial coordinate of the point particle trajectory $\mathbf{x}_1(\gamma_i)$ and $\mathbf{x}_2(\gamma_i)$ respectively. As required by the physical limit (discussed in section 2.3), we find that the values of the doubled degrees of freedom coincide at the critical point. The solution of the corresponding continuum geodesic equations, obtained via the LSODA algorithm of Mathematica's `NDSolve` command is shown as gray solid line and excellent agreement is observed. Note that due to our choice of $\dot{t}_i = 1$ the maximum time traversed by the simulation is close to one.

At first sight it appears that an equidistant discretization of time in γ emerges, but an inspection of the velocity of time with respect to γ in fig. 2 reveals that the time spacing dynamically adapts to the behavior observed in the spatial coordinate x . Close to the maximum of $x(\gamma)$ at around $\gamma = 0.4$ the temporal spacing e.g. has a minimum. This dynamically emerging time discretization constitutes an automatically generated non-trivial mesh for the time coordinate and arises naturally in our formalism. In fact an automatic AMR procedure results.

Let us plot next in fig. 3, the results from our geometrized formalism as physical trajectory, i.e. as $\mathbf{x}_{1,2}(t_{1,2})$ (red circles and blue crosses). This allows us to compare the outcome to the solution one would obtain by following the conventional approach in the literature (see e.g. chapter 7.9 in [1]). There one considers time as independent variable and simply adds a potential term to the free relativistic action eq. (2) before deriving the corresponding Euler-Lagrange equation, which for the linear potential reads $d^2x/dt^2 = -(\alpha)(1 - (dx/dt)^2)^{(3/2)}$. Using the LSODA algorithm of Mathematica's `NDSolve` command, we compute the solution of this equation of motion and plot it as gray solid line. Excellent agreement with the solution from our variational approach is observed, indicating that the geometrization strategy indeed reproduces the solution of the physical problem at hand.

Note that the change in the velocity of the time coordinate manifests itself here as a slightly denser time grid around the maximum of the trajectory.

After this qualitative visual inspection, let us take a closer look at the properties of the obtained solution. The first question we may ask is how well quantitatively the solution follows the naively discretized geodesic equations for time eq. (18) and space eq. (19) respectively. The *continuum* geodesic equations for the system at



hand read

$$\frac{d}{d\gamma} \left(g_{00} \frac{dt}{d\gamma} \right) = \frac{d}{d\gamma} \left((1 + 2\alpha x) \frac{dt}{d\gamma} \right) = 0, \quad (45)$$

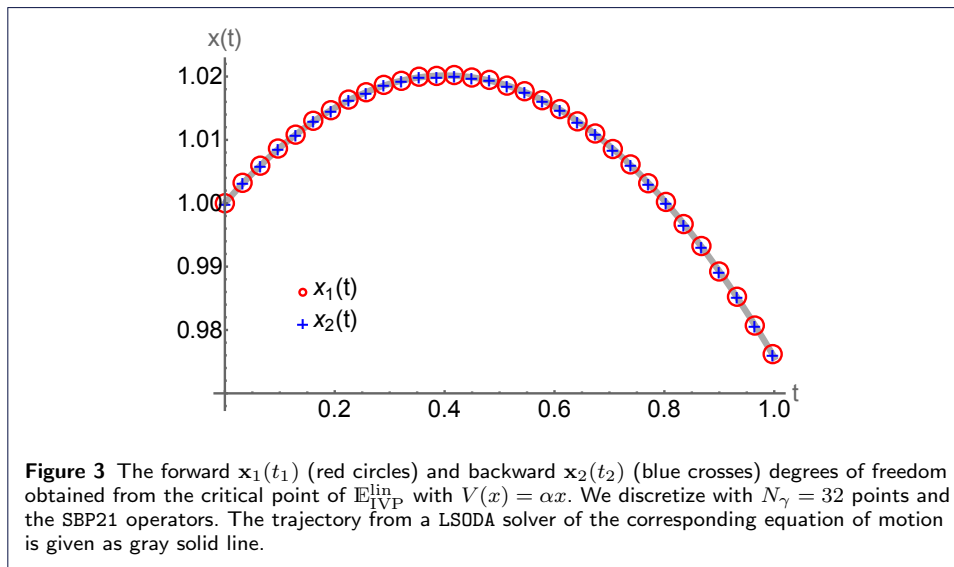
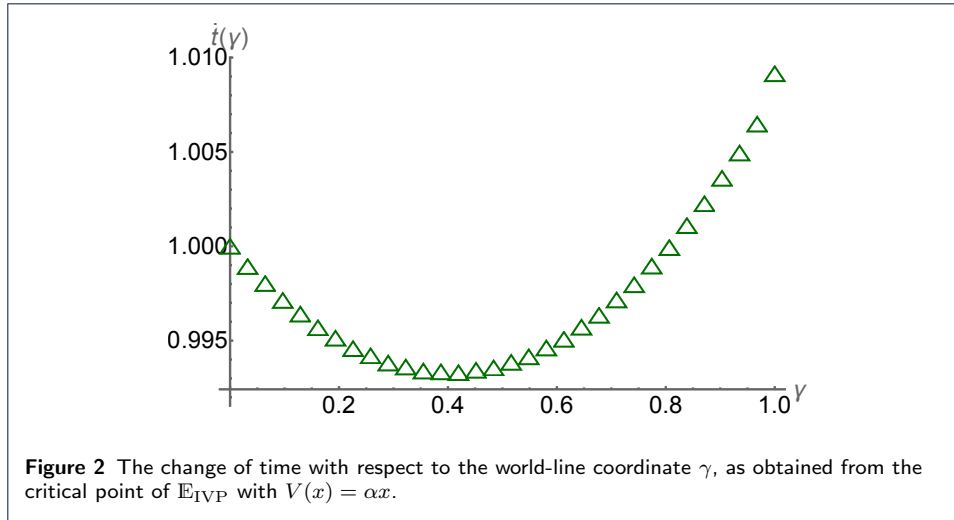
$$\frac{d}{d\gamma} \left(\frac{dx}{d\gamma} \right) + \frac{1}{2} \frac{\partial g_{00}}{\partial x} \left(\frac{dt}{d\gamma} \right)^2 = \frac{d^2 x}{d\gamma^2} + \alpha \left(\frac{dt}{d\gamma} \right)^2 = 0. \quad (46)$$

When deriving these equations of motion from the continuum action functional eq. (28) we have only used integration by parts. This motivates us to proceed, considering them naively discretized by replacing the derivatives with SBP finite difference operators

$$\mathbb{D}((1 + 2\alpha x) \circ (\mathbb{D}t)) = \Delta \mathbf{G}^t, \quad (47)$$

$$\mathbb{D}\mathbb{D}x + \alpha(\mathbb{D}t) \circ (\mathbb{D}t) = \Delta \mathbf{G}^x. \quad (48)$$

Here element-wise multiplication of entries of vector quantities is explicitly denoted by the symbol \circ , which implements e.g. $\mathbf{x}_1 \circ \mathbf{x}_2 = (x_1(0)x_2(0), x_1(\Delta\gamma)x_2(\Delta\gamma), \dots, x_1(\Delta\gamma(N_\gamma - 1))x_2(\Delta\gamma(N_\gamma - 1)))^T$. Note that we have introduced on the right of the above equations two quantities $\Delta \mathbf{G}^x$ and $\Delta \mathbf{G}^t$, which denote the deviation from the value

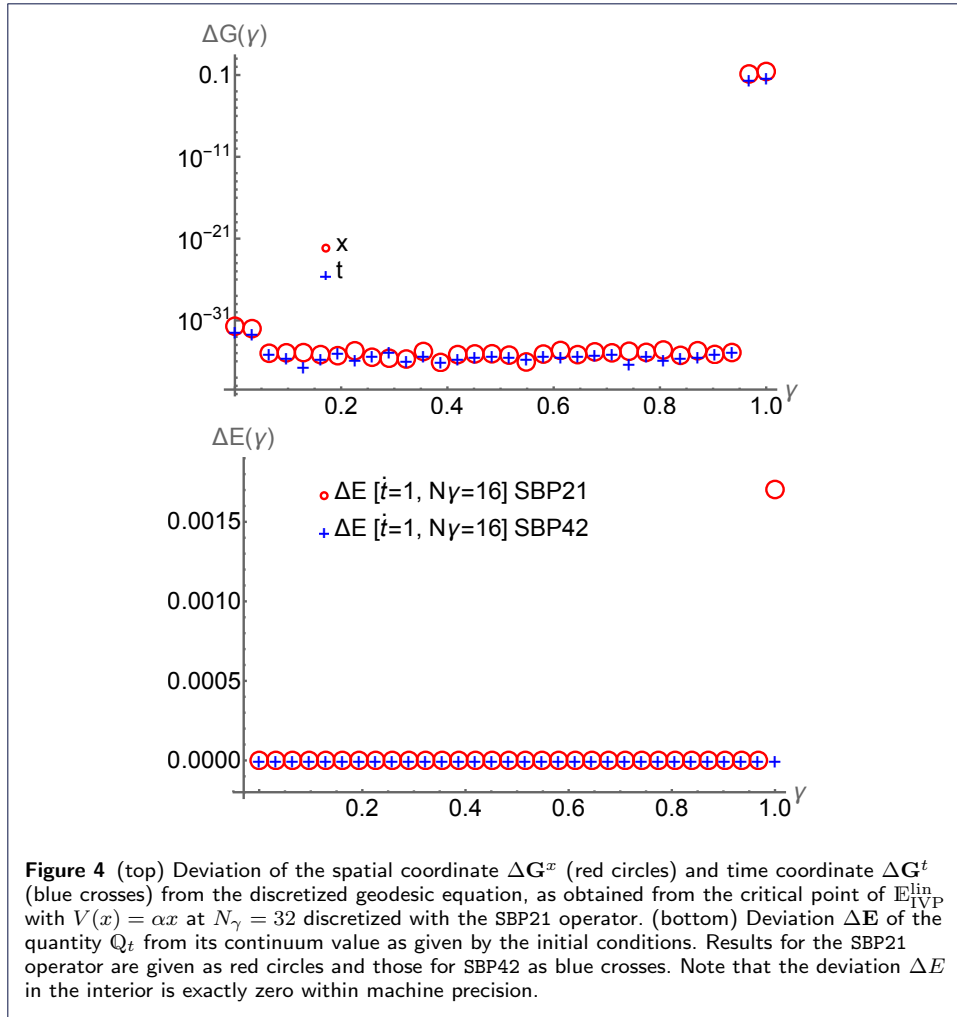


zero, to which the equations of motion evaluate in the continuum. By inspecting $\Delta \mathbf{G}^x$ and $\Delta \mathbf{G}^t$ for the trajectories $\mathbf{x}_{1,2}$ and $\mathbf{t}_{1,2}$ obtained from the critical point of the discretized action functional $\mathbb{E}_{\text{IVP}}^{\text{lin}}$, we can obtain first quantitative insight into the performance of our variational approach.

We plot the values of both quantities $\Delta \mathbf{G}^x$ and $\Delta \mathbf{G}^t$ in the top panel of fig. 4. At first sight we find that deviations from the naively discretized geodesic equations are minute, except for the two last points. Note that the plot is given in logarithmic scale.

Since we use a minimizer in Mathematica with `WorkingPrecision` set to 40, the values of $< 10^{-30}$ reflect a true zero. It is apparent that both the naively discretized geodesic equation for x and t are fulfilled down to machine precision.

Let us proceed to the central quantity of interest in this study Q_t , defined in eq. (22), which in the continuum represents the conserved quantity associated with the time-translation symmetry of the system. We again consider its naively dis-



cretized form in the following

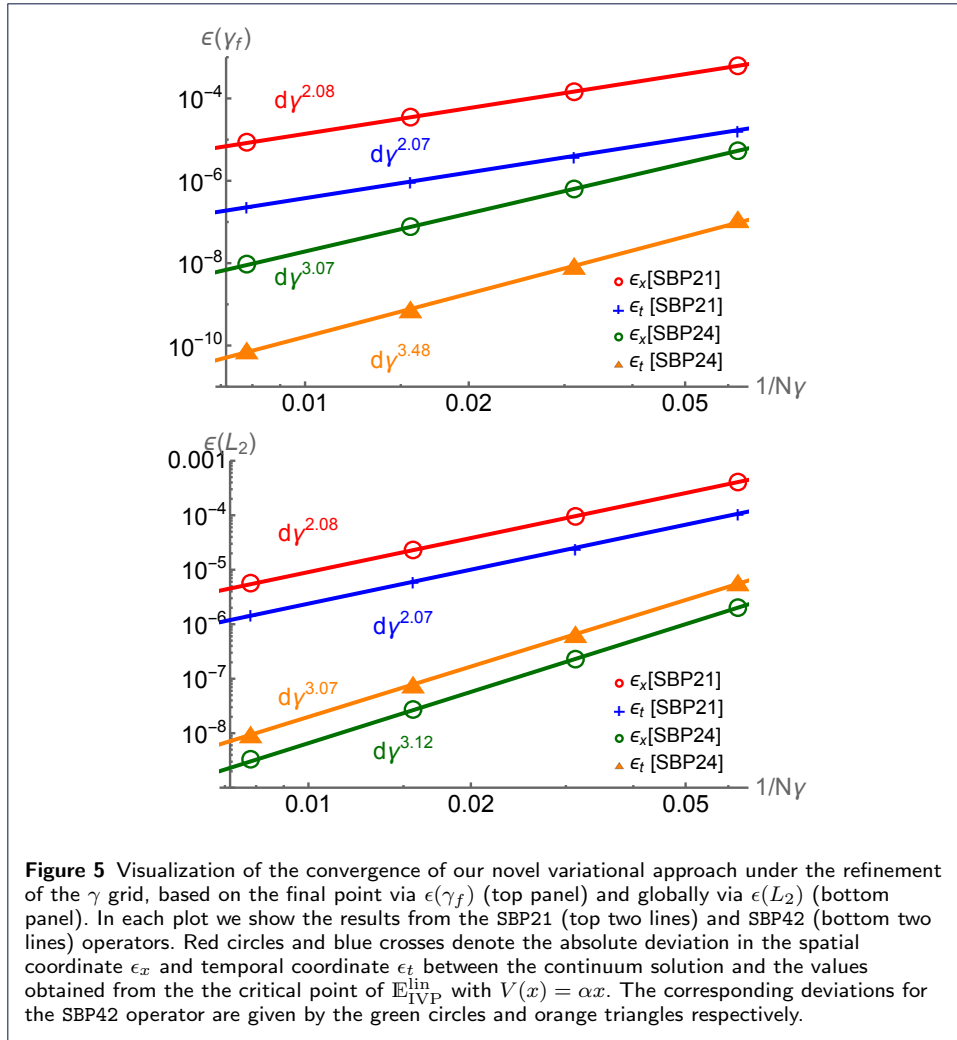
$$Q_t = (\mathbb{D}\mathbf{t}) \circ (\mathbf{1} + 2\alpha\mathbf{x}). \quad (49)$$

With the discrete action functional E_{IVP}^{lin} retaining manifest invariance under shifts in the time coordinates $\mathbf{t}_{1,2}$ we wish to investigate whether also the discretized Q_t retains its role as conserved Noether charge. To this end let us focus here on the deviation ΔE of Q_t from its continuum value

$$\Delta E = Q_t - Q_t = (\mathbb{D}\mathbf{t}) \circ (\mathbf{1} + 2\alpha\mathbf{x}) - \dot{t}_i(1 + 2\alpha x_i). \quad (50)$$

Note that Q_t takes on the continuum value by construction at the first point in γ , as there it is defined by the initial conditions. The values obtained for ΔE from the critical point of E_{IVP}^{lin} using either the SBP21 (red circles) or SBP42 operator (blue crosses) are shown in the bottom panel of fig. 4. There are two important observations to be made.

First, the discretized quantity Q_t is *exactly conserved* in the discrete setting in the *interior* of the simulated time domain and only at the final point γ_f it deviates



from that constant. While the deviation $\Delta \mathbf{E}(\gamma_f)$ in case of the SBP21 operator is already smaller than two permille, it reduces even further to a value of 10^{-6} when deploying the SBP42 operator.

We have investigated various potential reasons for the slight difference at the final point, such as a potential over-constraint from the connecting conditions in eqs. (31) and (35), but we have not identified the source as of yet. One venue to explore in the future is whether the exact enforcement of the connecting conditions plays a role, which however requires the development of a genuinely weak formulation of our approach without the use of Lagrange multipliers. It is important to point out that, as we will show explicitly below, the presence of this final differing point does not spoil the convergence to the correct continuum limit.

Secondly, the value of Q_t that remains conserved in the interior agrees with the true continuum value, prescribed by the initial conditions, *within machine precision*. This is a highly non-trivial result, as even in energy preserving schemes, such as the leap-frog, the conserved quantities do not necessarily agree with the continuum ones.

We surmise that it is the interplay of a manifest time-translation invariant formulation of the action functional, together with the resulting dynamically emerging time discretization, which achieves the conservation of the discrete Q_t at its continuum value in the interior of the simulation domain.

The presence of two points that deviate from the naively discretized continuum geodesic equations may appear troublesome. However as we show in fig. 5 these points do not spoil the convergence to the correct continuum limit under grid refinement.

In the top panel of fig. 5, we select the apparently most disadvantageous points for our convergence study, i.e. we compare the deviation from the continuum geodesic equations $\epsilon(\gamma_f)_x = |\mathbf{x}[N_\gamma] - x_{\text{true}}(1)|$ and $\epsilon(\gamma_f)_t = |\mathbf{t}[N_\gamma] - t_{\text{true}}(1)|$ at γ_f , exactly where the deviation from the continuum result was maximal in the top panel of fig. 4. Grid refinement is carried out and we provide the results for both the lowest order SBP21 operator and the next higher SBP42 operator.

Even in this disadvantaged scenario, we find that under grid refinement, the discrete solution approaches the true continuum values as expected from a scheme that is second order in the interior. Taking the SBP21 results, the best fit to ϵ_x reveals a scaling with $\Delta\gamma^{2.08}$, while for ϵ_t an virtually identical $\Delta\gamma^{2.07}$ ensues. Going over to the SBP42 results we find that the convergence is in line with expectations for an SBP operator of 4th order in the interior with ϵ_x exhibiting a scaling of $\Delta\gamma^{3.07}$ and ϵ_t a somewhat better value of $\Delta\gamma^{3.48}$.

In the bottom panel of fig. 5 we instead investigate the global convergence of our approach using the L_2 norm $\epsilon(L_2)_x = \sqrt{(\mathbf{x} - \mathbf{x}_{\text{true}})^T \cdot \mathbb{H} \cdot (\mathbf{x} - \mathbf{x}_{\text{true}})}$ and $\epsilon(L_2)_t = \sqrt{(\mathbf{t} - \mathbf{t}_{\text{true}})^T \cdot \mathbb{H} \cdot (\mathbf{t} - \mathbf{t}_{\text{true}})}$, where \mathbf{x}_{true} and \mathbf{t}_{true} are taken from the numerical solution of the geodesic equations, used for comparison in fig. 3. We find that similar convergence rates ensue, where SBP21 shows scaling $\Delta\gamma^\beta$ with exponent $\beta \geq 2$ and SBP42 shows scaling with exponent $\beta \geq 3$.

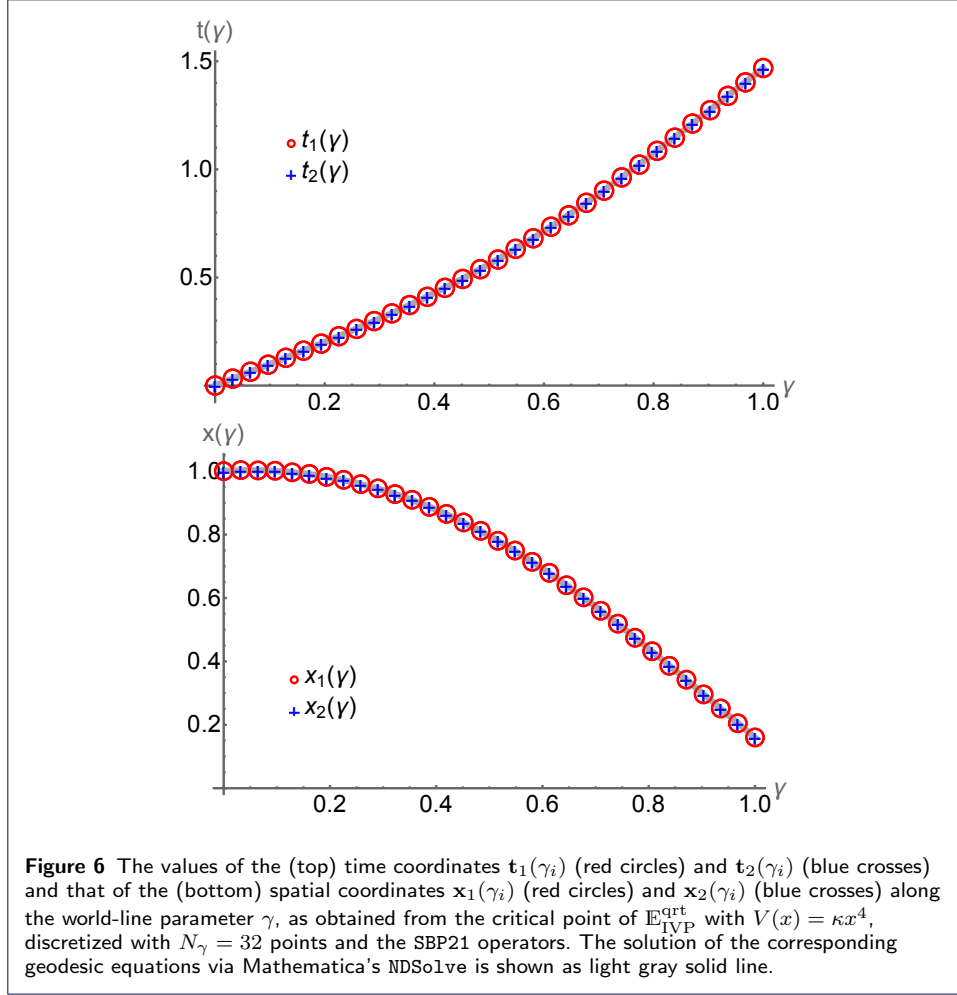
These convergence result agrees with the findings of our previous study [20], where the standard action functional was discretized with time as independent parameter.

4.2 Quartic potential

After considering the simplest possible non-trivial scenario with a linear potential, we now turn to a system with a quartic potential and the following continuum action functional

$$\begin{aligned} \mathcal{E}_{\text{IVP}}^{\text{qrt}} = & \int_{\gamma_i}^{\gamma_f} d\gamma \frac{1}{2} \left\{ \left(1 + 2\kappa x_1^4(\gamma)\right) \left(\frac{dt_1}{d\gamma}\right)^2 - \left(\frac{dx_1}{d\gamma}\right)^2 \right\} \\ & - \int_{\gamma_i}^{\gamma_f} d\gamma \frac{1}{2} \left\{ \left(1 + 2\alpha x_2^4(\gamma)\right) \left(\frac{dt_2}{d\gamma}\right)^2 - \left(\frac{dx_2}{d\gamma}\right)^2 \right\} \\ & + \lambda_1(t(\gamma_i) - t_i) + \lambda_2(\dot{t}_1(\gamma_i) - \dot{t}_i) + \lambda_3(x_1(\gamma_i) - x_i) + \lambda_4(\dot{x}_1(\gamma_i) - \dot{x}_i) \\ & + \lambda_5(t_1(\gamma_f) - t_2(\gamma_2)) + \lambda_6(\dot{t}_1(\gamma_f) - \dot{t}_2(\gamma_2)) \\ & + \lambda_7(x_1(\gamma_f) - x_2(\gamma_2)) + \lambda_8(\dot{x}_1(\gamma_f) - \dot{x}_2(\gamma_2)). \end{aligned} \quad (51)$$

Again we discretize along $N_\gamma = 32$ in the world-line parameter γ . Using $\kappa = 1/2$ in the potential $V(x) = \kappa x^4$ leads to dynamics that already in the small time regime considered here are distinctly anharmonic.

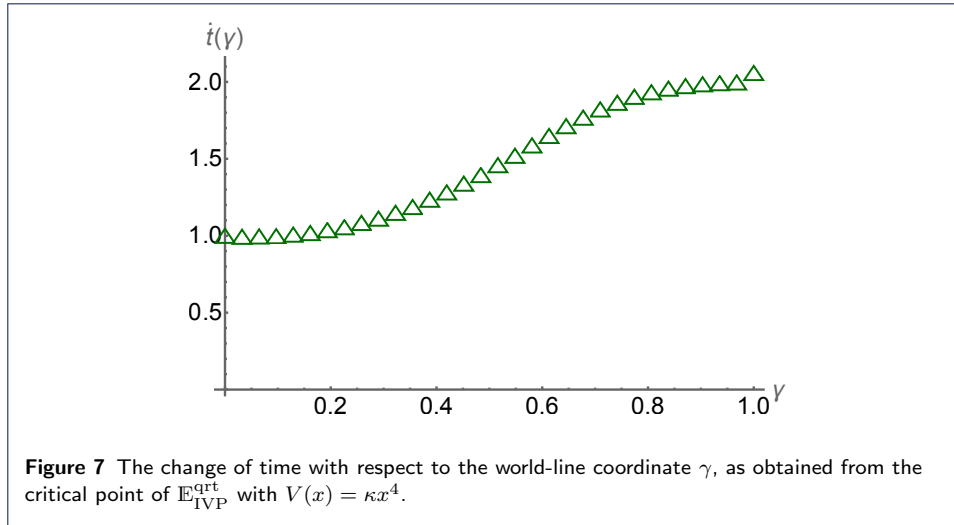


As in the previous subsection we discretize the world-line of the particle motion between $\gamma_i = 0$ and $\gamma_f = 1$, set the starting time to $t_i = 0$ and the starting position to $x_i = 1$. For our choice of $v_i = 1/10$ we again decide on $\dot{t} = 1$ and $\dot{x} = v_i$. The discretized action functional thus reads

$$\begin{aligned}
\mathbb{E}_{\text{IVP}}^{\text{qrt}} = & \frac{1}{2} \left\{ (\bar{\mathbb{D}}_t^R \mathbf{t}_1)^T \text{d} [1 + 2\kappa \mathbf{x}_1^4] \bar{\mathbb{H}}(\bar{\mathbb{D}}_t^R \mathbf{t}_1) - (\bar{\mathbb{D}}_x^R \mathbf{x}_1)^T \bar{\mathbb{H}}(\bar{\mathbb{D}}_x^R \mathbf{x}_1) \right\} \\
& - \frac{1}{2} \left\{ (\bar{\mathbb{D}}_t^R \mathbf{t}_2)^T \text{d} [1 + 2\kappa \mathbf{x}_2^4] \bar{\mathbb{H}}(\bar{\mathbb{D}}_t^R \mathbf{t}_2) - (\bar{\mathbb{D}}_x^R \mathbf{x}_2)^T \bar{\mathbb{H}}(\bar{\mathbb{D}}_x^R \mathbf{x}_2) \right\} \\
& + \lambda_1 (\mathbf{t}_1[1] - t_i) + \lambda_2 ((\mathbb{D} \mathbf{t}_1)[1] - \dot{t}_i) \\
& + \lambda_3 (\mathbf{x}_1[1] - x_i) + \lambda_4 ((\mathbb{D} \mathbf{x}_1)[1] - \dot{x}_i) \\
& + \lambda_5 (\mathbf{t}_1[N_\gamma] - \mathbf{t}_2[N_\gamma]) + \lambda_6 (\mathbf{x}_1[N_\gamma] - \mathbf{x}_2[N_\gamma]) \\
& + \lambda_7 ((\mathbb{D} \mathbf{t}_1)[N_\gamma] - (\mathbb{D} \mathbf{t}_2)[N_\gamma]) + \lambda_8 ((\mathbb{D} \mathbf{x}_1)[N_\gamma] - (\mathbb{D} \mathbf{x}_2)[N_\gamma]) \quad (52)
\end{aligned}$$

and taking the fourth power of the $\mathbf{x}_{1,2}$ vector is to be understood in an element wise fashion.

While for the linear potential, the time geodesic appeared to depend almost linearly on γ , we find that here a distinct curvature along γ emerges, as shown in



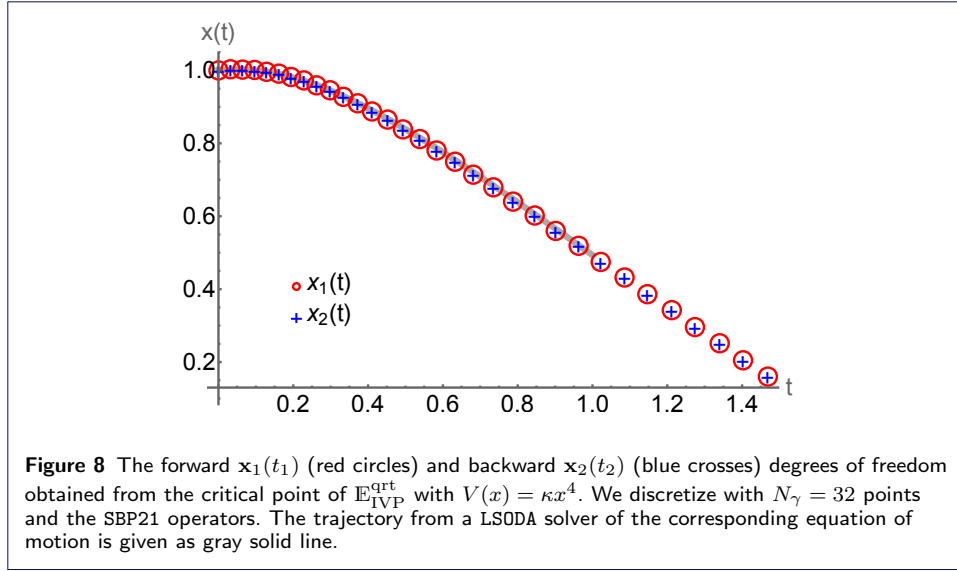
the top panel of fig. 6. We plot the values of $\mathbf{t}_1(\gamma_i)$ as red circles and $\mathbf{t}_2(\gamma_i)$ as blue crosses and show as gray solid line the solution of the corresponding geodesic equation, obtained from the LSODA algorithm of Mathematica's `NDSolve` command. Again the physical limit of equal values $\mathbf{t}_1(\gamma) = \mathbf{t}_2(\gamma)$ is realized.

The values of the spatial coordinate $\mathbf{x}_1(\gamma_i)$ and $\mathbf{x}_2(\gamma_i)$ as obtained from the critical point of $\mathbb{E}_{\text{IVP}}^{\text{qst}}$ with $V(x) = \kappa x^4$ are plotted in the bottom panel of fig. 6 with the direct numerical solution of the geodesic equation added as gray solid line.

Note that even though we have provided an initial velocity of the time along γ again with value $\dot{t}_i = 1$, the final time reached by the simulation now lies at $\mathbf{t}[N_\gamma] = 1.47$. Similarly one finds that a dynamical discretization in t emerges, which, as shown in fig. 7, varies from the initial values $\dot{t}_i = 1$ to $(\mathbb{D}\mathbf{t})[N_\gamma] = 2.06$. This behavior can be understood when realizing that the trajectory $x(t)$ in the non-linear case shows a stronger curvature close to $t = 0$ than at later times. I.e. we find again that the automatically generated non-trivial mesh (through automatic AMR) for the time coordinate adapts to the dynamics, by exhibiting a finer spacing at initial times.

Let us take a look at the results from our geometrized formalism as physical trajectory in fig. 8, i.e. plotted as $\mathbf{x}_{1,2}(t_{1,2})$ (red circles and blue crosses). They are compared to the solution of the conventional equation of motion, obtained from treating time as independent variable $d^2x/dt^2 = -(4\kappa x^3)(1 - (dx/dt)^2)^{(3/2)}$, computed via the LSODA algorithm of Mathematica's `NDSolve` command (gray solid line) in the range $t \in [0, 1]$. We find that within this range the solution from our geometrized discrete approach shows excellent agreement. Note that due to the non-equidistant emergent time discretization, the physical trajectory $x(t)$, shown in fig. 8 extends beyond the point $t = 1$.

As for the linear potential, let us investigate quantitatively the properties of the trajectories $\mathbf{t}(\gamma_i)$ and $\mathbf{x}(\gamma_i)$ by inserting them into the naively discretized geodesic equations. For the quartic potential, the continuum geodesic equations for the tem-



poral and spatial coordinate read

$$\frac{d}{d\gamma} \left(g_{00} \frac{dt}{d\gamma} \right) = \frac{d}{d\gamma} \left((1 + 2\kappa x^4) \frac{dt}{d\gamma} \right) = 0, \quad (53)$$

$$\frac{d}{d\gamma} \left(\frac{dx}{d\gamma} \right) + \frac{1}{2} \frac{\partial g_{00}}{\partial x} \left(\frac{dt}{d\gamma} \right)^2 = \frac{d^2 x}{d\gamma^2} + 4\kappa x^3 \left(\frac{dt}{d\gamma} \right)^2 = 0. \quad (54)$$

Naively discretizing these equations by replacing derivatives with SBP operators leads to the following discrete geodesic equations

$$\mathbb{D}((1 + 2\kappa \mathbf{x}^4) \circ \mathbb{D}\mathbf{t}) = \Delta \mathbf{G}^t, \quad (55)$$

$$\mathbb{D}\mathbb{D}\mathbf{x} + (4\kappa \mathbf{x}^3) \circ (\mathbb{D}\mathbf{t}) \circ (\mathbb{D}\mathbf{t}) = \Delta \mathbf{G}^x. \quad (56)$$

where again taking a power of the $\mathbf{x}_{1,2}$ vector is to be understood in an element wise fashion. To evaluate how well the solution obtained from the critical point of $\mathbb{E}_{\text{IVP}}^{\text{qrt}}$ fulfills the naive discretized geodesic equations we have again introduced the quantities $\Delta \mathbf{G}^t$ and $\Delta \mathbf{G}^x$ above.

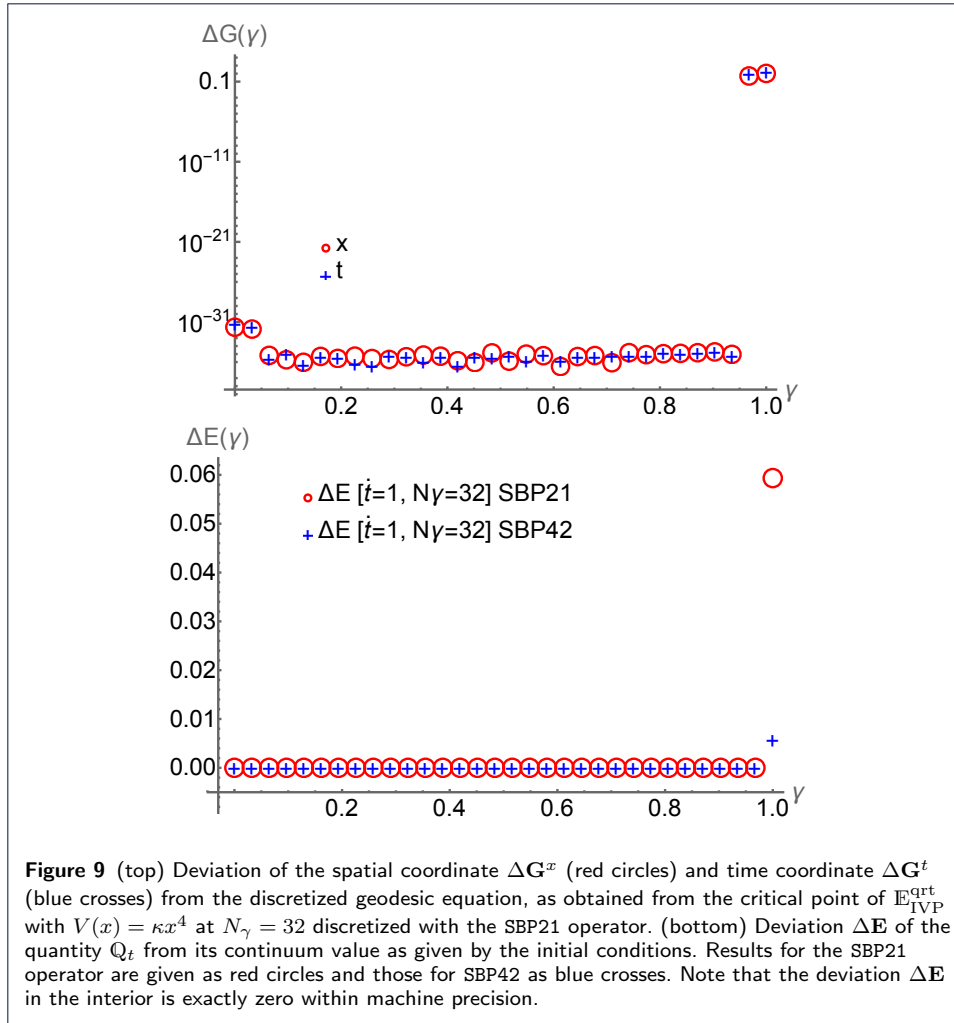
As shown in fig. 9 also here in the highly non-linear scenario, we find that the values of both \mathbf{x} (red circles) and \mathbf{t} (blue crosses) follow the discretized geodesic equations excellently, except for the last two points.

The most important question however remains whether in the non-linear discretized system, the continuum quantity Q_t from eq. (22) also remains conserved. Its naively discretized counterpart here reads

$$\mathbb{Q}_t = (\mathbb{D}\mathbf{t}) \circ (\mathbf{1} + 2\kappa \mathbf{x}^4), \quad (57)$$

and we define its deviation from the continuum result via the difference

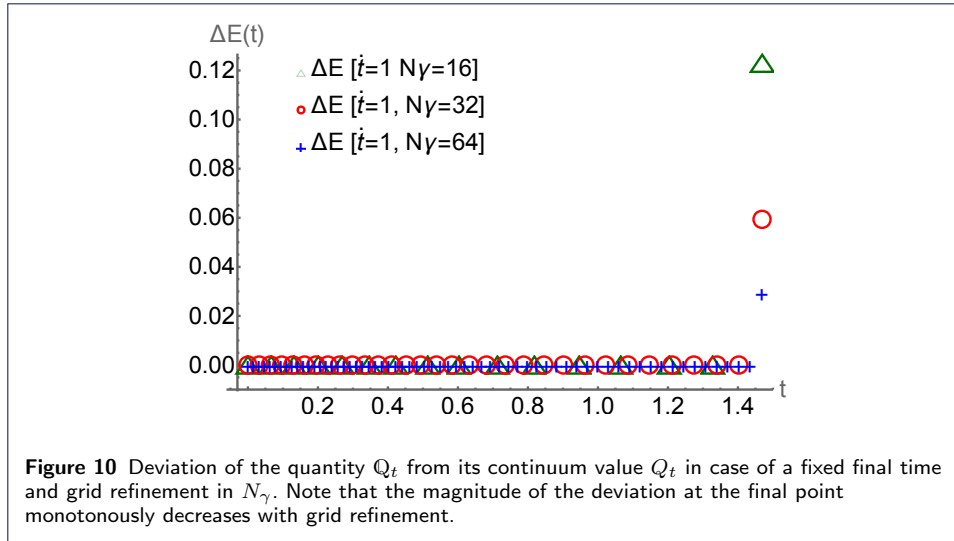
$$\Delta \mathbf{E} = \mathbb{Q}_t - Q_t = (\mathbb{D}\mathbf{t}) \circ (\mathbf{1} + 2\kappa \mathbf{x}^4) - \dot{t}_i (\mathbf{1} + 2\kappa x_i^4), \quad (58)$$



which we plot in the bottom panel of fig. 9 using the SBP21 operator (red circles) and the SBP42 operator (blue crosses).

We find also in the case of a non-linear potential that Q_t is preserved exactly in the interior of the simulation time domain. Up to machine precision its values in the interior also take on the correct continuum value. Similar to what we saw in the linear case, the last point deviates from the continuum value. It is reassuring to see that the absolute deviation at γ_f reduces already by an order of magnitude when going from a SBP21 to an SBP42 operator.

One may now ask whether the deviation of ΔE from its continuum value at γ_f is in some way related to the fact that we use $N_\gamma = 32$ points to discretize the world-line parameter. The answer is negative, as demonstrated in fig. 10. Three different datasets are shown in fig. 10, where for fixed \dot{t}_i the grid spacing in γ is changed. The green triangles denote the results for ΔE when using $N_\gamma = 16$, the red circles $N_\gamma = 32$ and the blue crosses $N_\gamma = 64$. We have confirmed explicitly that in all cases the values of Q_t are preserved up to machine precision in the interior of the simulated time domain. It is indeed only the last point that shows a deviation and we see that the absolute magnitude of the deviation reduces as the grid is refined.



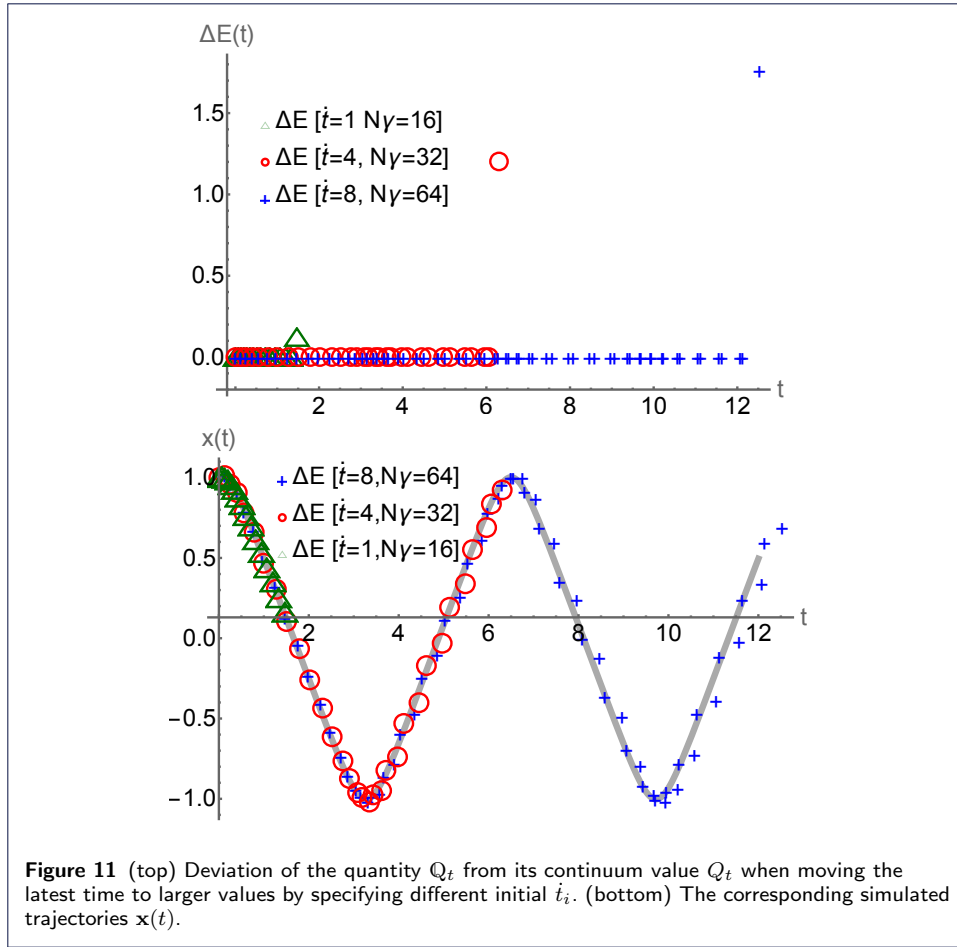
For the next test, we instead increase N_γ together with \dot{t}_i to let the simulation proceed to larger values of time t . In the top panel of fig. 11 we plot the deviation of Q_t from its continuum value for three choices $\dot{t}_i = 1, N_\gamma = 16$ (green triangles), $\dot{t}_i = 4, N_\gamma = 32$ (red circles) and $\dot{t}_i = 8, N_\gamma = 64$ (blue crosses). As seen before in the interior of the simulated time domain, the values of Q_t remain exactly preserved and only the last point deviates. We find that the magnitude of the deviation in the last point changes only marginally with the length of the simulated trajectory. For completeness the corresponding trajectories $x(t)$ are plotted in the bottom panel of fig. 11. Again let us emphasize that, as we will show below, the presence of this single deviating point does not spoil the convergence to the correct solution under grid refinement.

The exact conservation of the quantity Q_t in the interior is remarkable, as e.g. the trajectory in the bottom panel of fig. 11 for $\dot{t}_i = 8, N_\gamma = 64$ shows sizable discretization artifacts (which disappear under grid refinement). We believe that it is due to the manifest time-translation invariance of the underlying action functional that the combined dynamics of $x(\gamma)$ and $t(\gamma)$, including the automatically generated non-equidistant time mesh, achieve conservation of the continuum quantity.

The fact that the solutions we obtain fulfill the naively discretized geodesic equations and provide exact conservation of the continuum conserved charge in the interior of the simulated domain (see fig. 9) bodes well for establishing its stability. Since in the IVP setting $t(\gamma_f)$ is not given but emerges dynamically we cannot directly apply eq. (26) as proof of stability. However, as long as we can assume that the simulated time range (given a certain $\dot{t}(\gamma_i)$ is finite, the linear bound of eq. (26) on the norm \mathcal{H}_{BVP} holds in the discrete setting. In turn we deduce that the solution cannot exhibit stronger than linear rise of the derivatives of either $t(\gamma)$ or $x(\gamma)$, implying stability of the approach.

Let us now quantify the convergence properties of our variational approach using the results from the lowest order SBP21 operator and those coming from the SBP42 operator in fig. 12.

As in the linear potential case, in the top panel of fig. 12, we select the most disadvantageous points for our convergence study, i.e. we compare the deviation



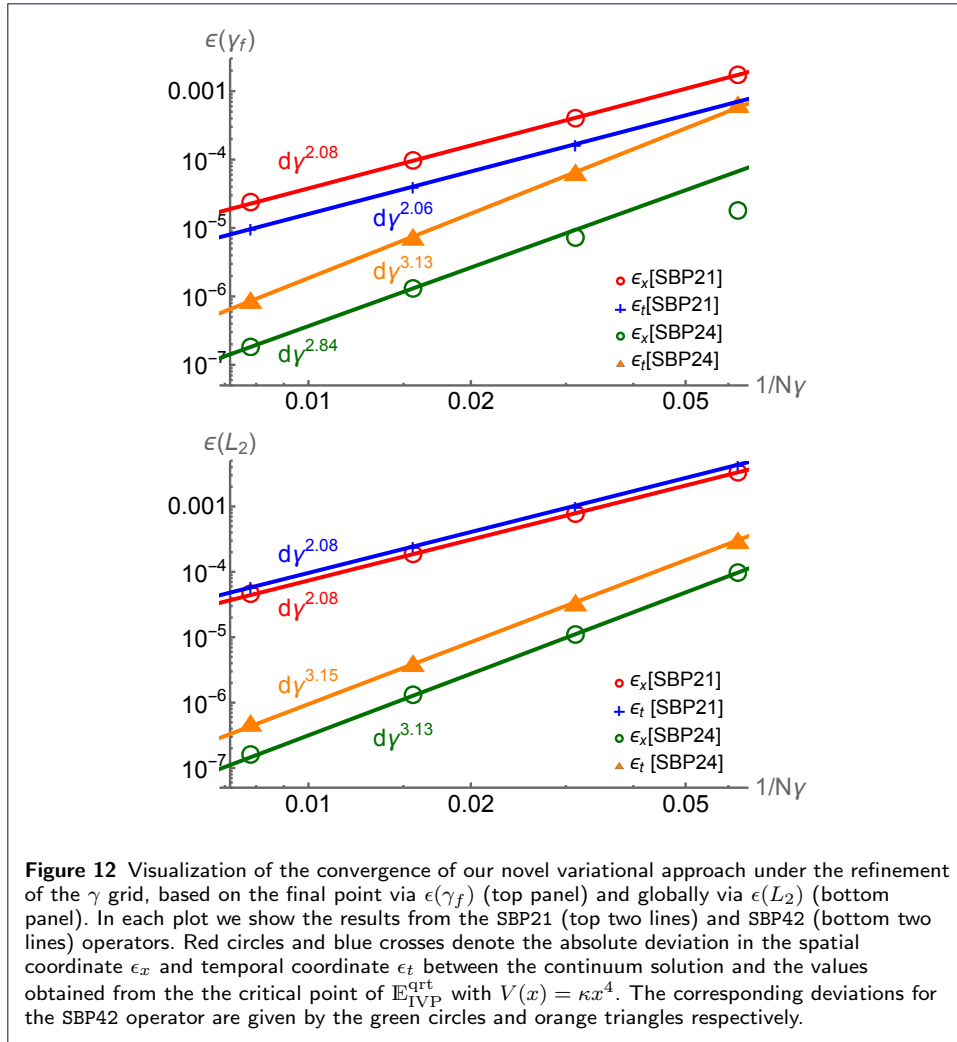
from the continuum geodesic equations $\epsilon(\gamma_f)_x = |\mathbf{x}[N_\gamma] - x_{\text{true}}(1)|$ and $\epsilon(\gamma_f)_t = |t[N_\gamma] - t_{\text{true}}(1)|$ at γ_f , exactly where the deviation from the continuum result was maximal in the top panel of fig. 9. Also in the non-linear scenario we find that under refinement of the γ grid, the discrete solution monotonously approaches the true continuum values.

Taking the SBP21 results, the best fit to $\epsilon(\gamma_f)_x$ reveals a scaling with $\Delta\gamma^{2.08}$, while for $\epsilon(\gamma_f)_t$ an virtually identical $\Delta\gamma^{2.06}$ is obtained.

For SBP42, we find that the convergence is slightly worse than in the linear potential case. As seen in the green circles plotted in fig. 12, the asymptotic convergence regime is reached for $32 < N_\gamma < 64$. Once we are in that regime, we find that $\epsilon(\gamma_f)_x$ exhibits a scaling of $\Delta\gamma^{2.84}$, close to the expected value of three. On the other hand $\epsilon(\gamma_f)_t$ shows a consistent performance with a scaling of $\Delta\gamma^{3.13}$ already at $N_\gamma = 32$.

Let us now investigate the global convergence in the bottom panel of fig. 12 using the L_2 norm $\epsilon(L_2)_x = \sqrt{(\mathbf{x} - \mathbf{x}_{\text{true}})^T \cdot \mathbb{H} \cdot (\mathbf{x} - \mathbf{x}_{\text{true}})}$ and correspondingly $\epsilon(L_2)_t = \sqrt{(t - t_{\text{true}})^T \cdot \mathbb{H} \cdot (t - t_{\text{true}})}$, where \mathbf{x}_{true} and t_{true} are taken from the numerical solution of the geodesic equations, used for comparison in fig. 6.

Reassuringly we find that the global convergence properties of our approach are better than indicated by those of the most disadvantaged point in the top panel of fig. 12. Indeed we find that for the SBP41 operators, the global scaling regime is reached already at $N_\gamma = 32$, similarly to the SBP21 case. In addition, the global



convergence rate $\Delta\gamma^\beta$ for SBP42 operators lies consistently above $\beta \geq 3$ for both the x and t degrees of freedom.

Again, these convergence result are in good agreement with those of our previous study [20], where the standard action functional was discretized with time as independent parameter.

5 Summary and Outlook

In this study we have put forward a novel geometric variational approach for solving a large class of initial value problems, associated with the dynamics of point particles evolving under a generic x dependent potential $V(x)$. Taking inspiration from the general theory of relativity, we consider both time and spatial coordinates of the point particle as dependent variables of a world-line parameter γ . We select a continuum action functional, which in the non-relativistic limit reduces to the standard action of point mechanics and whose critical point encodes a set of geodesic equations for $x(\gamma)$ and $t(\gamma)$. After doubling the degrees of freedom $t_{1,2}$ and $x_{1,2}$ we can relate the critical point of the corresponding doubled d.o.f. action with

the classical trajectory. Using the concept of Killing vectors we identify conserved quantities, e.g. related to the continuum time translation invariance of the action.

Deploying the regularized SBP operators originally introduced in [20], we discretize the continuum action and add Lagrange multipliers to enforce the initial and connecting conditions between the doubled $\mathbf{t}_{1,2}$ and $\mathbf{x}_{1,2}$. The main novelty of our approach is that the discretized action *retains the continuum symmetries*, in particular the invariance under time translations. Exactly mimicking integration by part through the use of SBP finite difference operators entails that the derivation of the conserved charges associated with the Killing vectors of the system is also exactly mimicked in the discrete setting. I.e. the continuum conserved quantities Q_K retain their role even after discretization.

The numerical results we obtain for both a linear and highly non-linear potential show that a discretization of time t now indeed emerges dynamically, adapting to the behavior of the spatial coordinate x . This is a concrete realization of an automatically generated non-equidistant mesh for the time coordinate, guided by our action functional with manifest continuum translation symmetry, i.e. an automatic AMR procedure. We have shown that except for the last two points along the discrete γ , the solution we obtain follows the naively discretized geodesic equations excellently.

Even more importantly, the naively discretized counterpart Q_t of the continuum conserved quantity Q_t *remains exactly preserved* in the interior of the simulated time domain, where it even *retains its continuum value* exactly within machine precision. A small deviation from the values in the interior for Q_t is observed at the last step γ_f . This deviation however decreases both under grid refinement, as well as when increasing the order of the SBP operator.

Point-wise, as well as global scaling analyses under grid refinement show that even in the presence of two points deviating from the naively discretized geodesic equations at the last two γ steps, the solution monotonously improves and manages to approach the true solution. When deploying the SBP21 operator, we achieve consistent scaling in $\Delta\gamma^\beta$ with $\beta \gtrsim 2$ for both the linear and non-linear potential. For SBP42 in case of a linear potential the dependence on the grid spacing follows the expected power law $\Delta\gamma^\beta$ with $\beta \gtrsim 3$ for all values of N_γ we inspected. For the non-linear potential, the scaling regime for point-wise convergence at the last point γ_f is reached with SBP42 for $32 < N_\gamma < 64$ with a slightly worse scaling of $2.84 \leq \beta \leq 3.13$. Global convergence on the other hand shows consistent scaling at all N_γ we considered, with exponents $\beta \geq 3$, in agreement with the findings in our previous paper [20], where the standard action functional was discretized with time as independent variable.

This study presents a proof of principle that initial value problems can be discretized, while retaining continuum symmetries. Three future directions will be explored: we may ask how we can capture systems of ordinary differential equations that e.g. contain a term that is proportional to a first derivative in x with respect to time? To this end we must exploit the versatility of the doubled d.o.f. approach more thoroughly. Furthermore we will explore how the reparametrization invariant formulation can be applied to partial differential equations in higher dimensions, taking insight from how the non-relativistic action emerges from our relativistic

starting point in eq. (8). In addition, to better understand the origin of the single deviating value in the otherwise exactly preserved Q_t , we will develop a genuinely weak formulation of our approach, devoid of Lagrange multipliers for enforcing initial and connecting conditions.

We believe that the quest for retention of defining continuum properties in discretized systems is both conceptually and practically valuable. Not only does the preservation of symmetries place powerful physical constraints on the solution but in addition offers a mechanism for the automatic generation of optimal discrete spacetime grids to ensure conservation of the Noether charges associated with these symmetries. We hope that this study provides the community with a novel impulse in this direction.

Acknowledgements

A. R. thanks Will Horowitz for inspiring and insightful discussions and Alex Nielsen for valuable insight on the general theory of relativity. A. R. gladly acknowledges support by the Research Council of Norway under the FRIPRO Young Research Talent grant 286883. J. N. was supported by the Swedish Research Council grant nr. 2021-05484. The study has benefited from computing resources provided by UNINETT Sigma2 - the National Infrastructure for High Performance Computing and Data Storage in Norway under project NN9578K-QCDrtX "Real-time dynamics of nuclear matter under extreme conditions"

Appendix A: Regularized SBP operators in affine coordinates

We here briefly review the idea and some technical aspects of constructing null-space consistent regularized SBP operators using affine coordinates, developed in our study [20].

The goal of regularizing conventional SBP operators \mathbb{D} , such as those defined e.g. in eq. (38) and eq. (39), lies in removing their unphysical zero modes. These may appear as highly oscillatory eigenfunctions to \mathbb{D}^T with zero eigenvalue. To this end we take inspiration from regularization techniques developed for partial differential equations. There the concept of null-space consistent SBP operators has been discussed in detail (see e.g. [38–41]).

For a differential equation, the boundary conditions may be enforced in the weak sense by adding a simultaneous approximation penalty term (SAT) [36], which can be partially absorbed into the finite difference operator, lifting its zero modes. Take for example a simple discretized first order differential equation

$$\mathbb{D}\mathbf{u} = \lambda\mathbf{u} + \sigma_0\mathbb{H}^{-1}\mathbb{E}_0(\mathbf{u} - \mathbf{g}), \quad (59)$$

where the SAT penalty term has been added to the right-hand side. It features the matrix $\mathbb{E}_0 = \text{diag}[1, 0, \dots, 0]$ that makes reference only to the first entry in the discretized functions \mathbf{u} and \mathbf{g} , the latter of which contains the initial value in its first entry $\mathbf{g} = (u_0, 0, \dots, 0)$. The SAT term also contains \mathbb{H}^{-1} , i.e. Δt^{-1} , which increases the strength of the penalty as $\Delta t \rightarrow 0$. The parameter σ_0 in the SBP-SAT approach is tuned to satisfy stability properties and its optimal value is found to be $\sigma_0 = -1$ (see e.g. ref. [42–44]), a choice we adopt in the following. In the differential

equation context one conventionally absorbs the term proportional to \mathbf{u} into a new $\bar{\mathbb{D}} = \mathbb{D} - \sigma_0 \mathbb{H}^{-1} E_0$. This new operator is devoid of zero modes [45] and may be inverted to obtain the solution \mathbf{u} .

In the context of an action functional, such as eq. (42), we do not have an equal sign around which we can move the SAT term. Instead we must incorporate the whole of the penalty term directly in a modified SBP operator. Since the penalty term in our example eq. (59) contains both a contribution that is proportional to the function \mathbf{u} and a constant shift \mathbf{g} it amounts to an affine transformation on \mathbf{u} , which can be captured efficiently using affine coordinates. To this end let us write $\bar{A}[\mathbf{b}]\bar{\mathbf{x}} = A\mathbf{x} + \mathbf{b}$, where $\bar{A}[\mathbf{b}]$ refers to a matrix A extended by an additional row and column with the value 1 placed in the lower right corner. The new column available in $\bar{A}[\mathbf{b}]$ is populated with the entries of \mathbf{b} . The vector $\bar{\mathbf{x}}$ is nothing but \mathbf{x} extended by one more entry with value unity. We will use this construction principle to define a regularized $\bar{\mathbb{D}}$ from our conventional SBP operator \mathbb{D} .

Since we have both \mathbf{x} and \mathbf{t} as independent degrees of freedom each with independent initial conditions x_i and t_i , we must define different shifts \mathbf{b}^x and \mathbf{b}^t respectively and thus end up with two different regularized SBP operators $\bar{\mathbb{D}}_t$ and $\bar{\mathbb{D}}_x$. The shift terms are nothing but the constant part of the corresponding SAT term, absorbed into the SBP operator

$$\mathbf{b}^x = \sigma_0 \mathbb{H}^{-1} E_0 \mathbf{g}^x, \quad \mathbf{b}^t = \sigma_0 \mathbb{H}^{-1} E_0 \mathbf{g}^t. \quad (60)$$

Here $\mathbf{g}^x = \text{diag}[x_i, 0, \dots, 0]$ and $\mathbf{g}^t = \text{diag}[t_i, 0, \dots, 0]$ encode the initial values for x and t respectively. As mentioned before, we choose the parameter $\sigma_0 = -1$, whenever a penalty term is incorporated in $\bar{\mathbb{D}}$, motivated by the fact that in the conventional treatment of IVPs using the SBP-SAT approach, this value leads to a minimal discretization error (see e.g. ref. [42–44]). The resulting regularized SBP operators to be deployed on $\mathbf{t}_{1,2}$ or $\mathbf{x}_{1,2}$, are given explicitly in eq. (40) and eq. (41) respectively.

Consistent with the affine coordinates used in the newly defined $\bar{\mathbb{D}}_t$ and $\bar{\mathbb{D}}_x$, we also amend the discretized trajectories $\mathbf{t}_{1,2}$ and $\mathbf{x}_{1,2}$ by one more entry that is given the value one.

In order to compute inner products in the space of discretized functions, we also have to modify the quadrature matrix $\mathbb{H} \rightarrow \bar{\mathbb{H}}$ by amending it by one row and column filled with zeros. We do not include the value one in the lower right corner in order to correctly account for the fact that the vectors appearing as arguments to the inner product contain an auxiliary final entry, which does not contribute to the value of the inner product and only facilitates the efficient implementation of shift operations. For more details on the affine coordinate regularization technique see [20].

Competing interests

The authors declare that they have no competing interests.

Author's contributions

- A. Rothkopf: formulation of the geometric variational approach, literature review, numerical experiments, writing, editing
- J. Nordström: guidance on the formulation and implementation of SBP based discretization schemes, literature review, editing

Author details

¹Faculty of Science and Technology, University of Stavanger, 4021, Stavanger, Norway. ²Department of Mathematics, Linköping University, SE-581 83, Linköping, Sweden. ³Department of Mathematics and Applied Mathematics, University of Johannesburg, P.O. Box 524, Auckland Park 2006, Johannesburg, South Africa.

References

- Goldstein, H., Poole, C.P., Safko, J.L.: *Classical Mechanics*. Addison Wesley (2002)
- Arnold, V.I., Vogtmann, K., Weinstein, A.: *Mathematical Methods of Classical Mechanics*. Graduate Texts in Mathematics. Springer (2013)
- Coleman, S.: *Aspects of Symmetry: Selected Erice Lectures*. Cambridge University Press, Cambridge, U.K. (1985). doi:[10.1017/CBO9780511565045](https://doi.org/10.1017/CBO9780511565045)
- Noether, E.: Invariant variation problems. *Transport theory and statistical physics* **1**(3), 186–207 (1971)
- Landau, L.D., Lifshitz, E.M.: *The Classical Theory of Fields: Volume 2. Course of theoretical physics*. Elsevier Science (2000)
- Yanagihara, R., Iritani, T., Kitazawa, M., Asakawa, M., Hatsuda, T.: Distribution of Stress Tensor around Static Quark–Anti-Quark from Yang–Mills Gradient Flow. *Phys. Lett. B* **789**, 210–214 (2019). doi:[10.1016/j.physletb.2018.09.067](https://doi.org/10.1016/j.physletb.2018.09.067). [1803.05656](https://arxiv.org/abs/1803.05656)
- Cockburn, B., Karniadakis, G.E., Shu, C.-W.: *Discontinuous Galerkin Methods: Theory, Computation and Applications* vol. 11. Springer (2012)
- Svärd, M., Nordström, J.: Review of summation-by-parts schemes for initial–boundary-value problems. *Journal of Computational Physics* **268**, 17–38 (2014)
- Fernández, D.C.D.R., Hicken, J.E., Zingg, D.W.: Review of summation-by-parts operators with simultaneous approximation terms for the numerical solution of partial differential equations. *Computers & Fluids* **95**, 171–196 (2014)
- Lundquist, T., Nordström, J.: The SBP-SAT technique for initial value problems. *Journal of Computational Physics* **270**, 86–104 (2014)
- Nordström, J., Lundquist, T.: Summation-by-parts in time. *Journal of Computational Physics* **251**, 487–499 (2013)
- Nordström, J., Lundquist, T.: Summation-by-parts in time: the second derivative. *SIAM Journal on Scientific Computing* **38**(3), 1561–1586 (2016)
- Johnson, R.C.: Angular momentum on a lattice. *Physics Letters B* **114**(2), 147–151 (1982). doi:[10.1016/0370-2693\(82\)90134-4](https://doi.org/10.1016/0370-2693(82)90134-4)
- Regan, H.M.: Von neumann stability analysis of symplectic integrators applied to hamiltonian pdes. *Journal of Computational Mathematics* **20**(6), 611–618 (2002)
- Nordström, J.: *Nonlinear Boundary Conditions for Initial Boundary Value Problems with Applications in Computational Fluid Dynamics*. [2306.01297](https://arxiv.org/abs/2306.01297)
- Verlet, L.: Computer “Experiments” on Classical Fluids. I. Thermodynamical Properties of Lennard-Jones Molecules. *Physical Review* **159**(1), 98–103 (1967). doi:[10.1103/PhysRev.159.98](https://doi.org/10.1103/PhysRev.159.98). Publisher: American Physical Society
- Dirac, P.A.M.: Generalized Hamiltonian Dynamics. *Canadian Journal of Mathematics* **2**, 129–148 (1950). doi:[10.4153/CJM-1950-012-1](https://doi.org/10.4153/CJM-1950-012-1). Publisher: Cambridge University Press
- Anerot, B., Cresson, J., Hariz Belgacem, K., Pierret, F.: Noether’s-type theorems on time scales. *Journal of Mathematical Physics* **61**(11), 113502 (2020). doi:[10.1063/1.5140201](https://doi.org/10.1063/1.5140201). Number: 11
- Stephani, H.: *Relativity: An Introduction to Special and General Relativity*. Cambridge University Press (2004)
- Rothkopf, A., Nordström, J.: A new variational discretization technique for initial value problems bypassing governing equations. *J. Comput. Phys.* **477**, 111942 (2023). doi:[10.1016/j.jcp.2023.111942](https://doi.org/10.1016/j.jcp.2023.111942). [2205.14028](https://arxiv.org/abs/2205.14028)
- Berger, M.J., Olinger, J.: Adaptive mesh refinement for hyperbolic partial differential equations. *Journal of computational Physics* **53**(3), 484–512 (1984)
- Löhner, R.: An adaptive finite element scheme for transient problems in CFD. *Computer methods in applied mechanics and engineering* **61**(3), 323–338 (1987)
- Berger, M.J., Colella, P.: Local adaptive mesh refinement for shock hydrodynamics. *Journal of computational Physics* **82**(1), 64–84 (1989)
- Persson, P.-O., Peraire, J.: Sub-cell shock capturing for discontinuous Galerkin methods. In: 44th AIAA Aerospace Sciences Meeting and Exhibit, p. 112 (2006)
- Nemec, M., Aftosmis, M., Wintzer, M.: Adjoint-based adaptive mesh refinement for complex geometries. In: 46th AIAA Aerospace Sciences Meeting and Exhibit, p. 725 (2008)
- Offermans, N., Massaro, D., Peplinski, A., Schlatter, P.: Error-driven adaptive mesh refinement for unsteady turbulent flows in spectral-element simulations. *Computers & Fluids* **251**, 105736 (2023)
- Mavriplis, C.: Adaptive mesh strategies for the spectral element method. *Computer methods in applied mechanics and engineering* **116**(1-4), 77–86 (1994)
- Henderson, R.D.: Adaptive spectral element methods for turbulence and transition. In: *High-order Methods for Computational Physics*, pp. 225–324. Springer (1999)
- Kompenhans, M., Rubio, G., Ferrer, E., Valero, E.: Adaptation strategies for high order discontinuous Galerkin methods based on tau-estimation. *Journal of Computational Physics* **306**, 216–236 (2016)
- Galley, C.R.: Classical Mechanics of Nonconservative Systems. *Physical Review Letters* **110**(17), 174301 (2013). doi:[10.1103/PhysRevLett.110.174301](https://doi.org/10.1103/PhysRevLett.110.174301). Publisher: American Physical Society
- Jost, J., Li-Jost, X.: *Calculus of Variations*. Cambridge Studies in Advanced Mathematics. Cambridge University Press (1998)
- Carroll, S.M.: *Spacetime and Geometry*. Cambridge University Press (2019)
- Carlip, S.: *General Relativity: A Concise Introduction*. OUP Oxford (2019)
- Rizzuti, B.F., Júnior, G.F.V., Resende, M.A.: To square root the Lagrangian or not: an underlying geometrical analysis on classical and relativistic mechanical models. arXiv. arXiv:1905.01177 [math-ph, physics:physics]

- (2019). doi:[10.48550/arXiv.1905.01177](https://doi.org/10.48550/arXiv.1905.01177). <http://arxiv.org/abs/1905.01177>
35. Berges, J., Gasenzer, T.: Quantum versus classical statistical dynamics of an ultracold Bose gas. *Phys. Rev. A* **76**, 033604 (2007). doi:[10.1103/PhysRevA.76.033604](https://doi.org/10.1103/PhysRevA.76.033604). [cond-mat/0703163](https://arxiv.org/abs/cond-mat/0703163)
 36. Carpenter, M.H., Gottlieb, D., Abarbanel, S.: Time-stable boundary conditions for finite-difference schemes solving hyperbolic systems: Methodology and application to high-order compact schemes. *Journal of Computational Physics* **111**(2), 220–236 (1994)
 37. Rothkopf, A.: Mathematica 12 implementation of a symmetry and Noether charge preserving IVP discretization technique (2023). doi:[10.5281/zenodo.8129657](https://doi.org/10.5281/zenodo.8129657)
 38. Svärd, M., Nordström, J.: On the convergence rates of energy-stable finite-difference schemes. *Journal of Computational Physics* **397**, 108819 (2019)
 39. Linders, V., Nordström, J., Frankel, S.H.: Properties of Runge-Kutta-Summation-By-Parts methods. *Journal of Computational Physics* **419**, 109684 (2020). doi:[10.1016/j.jcp.2020.109684](https://doi.org/10.1016/j.jcp.2020.109684)
 40. Svärd, M., Nordström, J.: Convergence of energy stable finite-difference schemes with interfaces. *Journal of Computational Physics* **429**, 110020 (2021). doi:[10.1016/j.jcp.2020.110020](https://doi.org/10.1016/j.jcp.2020.110020)
 41. Ranocha, H., Nordström, J.: A new class of a stable summation by parts time integration schemes with strong initial conditions. *Journal of Scientific Computing* **87**(1), 1–25 (2021)
 42. Ålund, O., Nordström, J.: A provably stable, non-iterative domain decomposition technique for the advection-diffusion equation. Linköping University Electronic Press (2016)
 43. Ålund, O., Nordström, J.: Encapsulated high order difference operators on curvilinear non-conforming grids. *Journal of Computational Physics* **385**, 209–224 (2019). doi:[10.1016/j.jcp.2019.02.007](https://doi.org/10.1016/j.jcp.2019.02.007)
 44. Glaubitz, J., Nordström, J., Öffner, P.: Summation-by-parts operators for general function spaces. *SIAM Journal on Numerical Analysis* **61**(2), 733–754 (2023)
 45. Ruggiu, A.A., Nordström, J.: Eigenvalue Analysis for Summation-by-Parts Finite Difference Time Discretizations. *SIAM Journal on Numerical Analysis* **58**(2), 907–928 (2020). doi:[10.1137/19M1256294](https://doi.org/10.1137/19M1256294). Publisher: Society for Industrial and Applied Mathematics